Supplementary Information (SI) for Physical Chemistry Chemical Physics.
This journal is © the Owner Societies 2025
Please do not adjust margins

ARTICLE

SUPPORTING INFORMATION

Received 00th January 20xx,
Accepted 00th January 20xx

DOI: 10.1039/x0xx00000x

Gas-phase reactivity of hexanuclear molybdenum $[Mo_6I_{14}]^{2-}$ and its photo-fragments towards O_2 and CO_2: combined mass spectrometry (MS^n) and quantum chemical simulations

Aikaterini Tsirkou [a], Nina Tyminska [b,c], Richard A. J. O'Hair [d], Fabien Grasset [e], Yann Molard [c], Karine Costuas [*c], Stéphane Cordier [*c], Luke MacAleese [*a]

Table of content

Complements

S1 - Collision rate calculation details 3

S2 – Secondary fragments: full description and discussion 3

S3 – Details on the experimental optical spectroscopy method 5

S4 – Details on the COSMO correction 5

Tables

S0 - Peak list and integration windows for the analysis of $[Mo_6I_{14}]^{2-}$ action spectra in Figure 2 & Figure 3 6

S1 - Peak list, mass differences and assignments for MS in Figure 1 and Figure 6. 6

S2 - Peak list, mass differences and assignments for MS in Fig 11. 7

S3 - SCM-ADF energies ($E_{SCM-ADF}$), Gibbs free energies ($G_{SCM-ADF}$) and enthalpies ($H_{SCM-ADF}$) at 298 K of all ions and molecules calculated. 8

S4 - Gibbs free energies ($\Delta G_{298\,K}$) and enthalpies ($\Delta H_{298\,K}$) at 298 K of the indicated reaction. 17

Figures

S0 - Data analysis workflow for each wavelength range of acquisition: the fragmentation ratios (boxplots) are statistically analysed and medians are baseline corrected, then smoothed and ultimately corrected for the laser profile (divided by power*wavelength which is called here "instrument response function" or IRF). This workflow is applied to the 2 UV ranges and 2 replicates in the Visible range. **18**

S1 - CID spectrum of $[Mo_6I_{14}]^{1-}$ at *m/z* 2348 (formed by LID of precursor $[Mo_6I_{14}]^{2-}$). The exclusive activation product is marked with thick blue arrows and corresponds to the loss of radical iodine $I^{\bullet}$. **19**

[a] *Institut Lumière Matière, UMR5306 CNRS & UCBL, Lyon, France*
[b] *Institute for the Sciences of Light, University Paris-Saclay.*
[c] *Institut des Sciences Chimiques de Rennes, UMR6226 CNRS & Université de Rennes, Rennes, France.*
[d] *School of Chemistry and Bio21 Institute of Molecular Science and Biotechnology University of Melbourne, Victoria, Australia.*
[e] *CNRS–Saint-Gobain–NIMS, IRL3629, LINK, National Institute for Materials Science, Ibaraki, Japan*

Electronic Supplementary Information (ESI) available: [details of any supplementary information available should be included here]. See DOI: 10.1039/x0xx00000x

Please do not adjust margins

Please do not adjust margins

S2 - CID spectrum of $[Mo_6I_{13}]^{1-}$ at *m/z* 2223 (formed by ISD after ESI of a solution of $Cs_2Mo_6I_{14}$). **19**

S3 - CID spectrum of $[Mo_6I_{13}]^{2-\bullet}$ at *m/z* 1112 (formed by LID of precursor $[Mo_6I_{14}]^{2-}$. Primary activation products are marked with thick blue arrows. Secondary fragment series resulting from O_2 addition and $I^\bullet$ losses are indicated with orange and red scales. Mo_6 core fragmentation is observed as attested by several complex patterns in insets (the small isolation window enables to simulate exact patterns for specific neutral losses: see orange/purple patterns in inset). **20**

S4 - The representation of the frontier MOs of (Spin)orbital of $[Mo_6I_{14}]^{2-}$, $[Mo_6I_{14}]^{1-\bullet}$, $[Mo_6I_{13}]^{2-\bullet}$, and $[Mo_6I_{13}]^{-}$. The corresponding molecular energy diagrams are given in Figure 2 in the main text. = HOMO = highest occupied molecular orbitals; $HOSO_\alpha$ / $HOSO_\beta$ = highest occupied spin orbital α / β; LUMO = lowest unoccupied molecular orbital; $LUSO_\alpha$ / $LUSO_\beta$ = = lowest unoccupied spin orbital α / β. Isocontours = ±0.02 $(e.bohr^3)^{½}$. **21**

S5 - Spin-density representation of $[Mo_6I_{14}]^{1-\bullet}$ and $[Mo_6I_{13}]^{2-\bullet}$. Isocontours = ±0.0025 $e.bohr^3$. **21**

S6 - Photo-fragmentation spectrum (LID) at 260 nm of a single isotopic peak (*m/z* 847) of the precursor ion $Mo_6Br_{14}^{2-}$. LID mainly yields singly charged fragments resulting either from the electron photo-detachment or from the loss of I^-, both followed by successive I_2 losses. In comparison with the iodinated compound, the reduced dianion species $(6,13,0)^{2-\bullet}$ is not detected at *m/z* 807. **22**

S7 - IMR spectrum of $[Mo_6I_{14}]^{1-}$ at *m/z* 2348 (formed by LID of precursor $[Mo_6I_{14}]^{2-}$). No product is formed from reaction with trace O_2 (see Figure 7 for comparison with reactivity of (6,13,0)2- under similar conditions). **22**

S8 - IMR spectrum of $[Mo_6I_{13}]^{1-}$ at *m/z* 2223 (formed by LID of precursor $[Mo_6I_{14}]^{2-}$). No product is formed from reaction with trace O_2 (see Figure 7 for comparison with reactivity of (6,13,0)2- under similar conditions). **23**

S9 - Evolution of the photo-product ion $[Mo_6I_{13}]^{2-}$ (marked with asterix) after 250 ms in the trap background gas (He with unavoidable traces of O_2). Insets show ion series that all derive from an initial O_2 addition. Left and right insets display simulated isotope patterns in purple or orange for respectively $[MoI_2O_2]^{1-}$ and [selected precursor *m/z* - $MoI_2O_2]^{1-}$ or $[Mo_6I_{10}O_2]^{1-}$. **23**

S10 - Comparison of the oxidation ratio of clusters $(6,13,x)^{1-}$ (top) vs. $(6,13,x)^{2-\bullet}$ (middle) and $(6,12,0)^{1-\bullet}$ (bottom). Data is presented as relative ion counts per bin calculated over more than 3000 mass spectra recorded within the UV and optical absorption bands of $(6,14,0)^{1-}$. While $(6,13,x)^{1-}$ displays systematically strict zero ratios, a bi-modal distribution is observed for$(6,13,x)^{2-\bullet}$ which is comparable to $(6,12,x)^{1-\bullet}$. **24**

S11 - Reactivity of $(6,13,0)^{2-}$ at *m/z* 1112 with trap background gas. Top: Helium (with unavoidable traces of O_2); middle: He:O_2(0.5%); and bottom: He:CO_2(0.5%). **24**

S12 - Representation of the optimized geometry of (6,13,2)2-• and list of the interatomic distances**.** **25**

S13 - In source CID of $(6,14,0)^{2-}$ in presence of 0.5% CO_2 in the trapping gas. Major fragments correspond to $(6,n,2k)^{1-}$ species similar to what is observed with O_2 traces. No CO_2 adduct peak is directly identified. However, some *odd* oxygen ions are observed, *e.g.* at *m/z* 1543. **25**

S14 - CID-MS^2 spectrum of precursor species $(6,5,6)^{1-}$ formed by in-source CID (80 V) and isolated at m/z 1306. Collisional activation (NCE 22) was applied during 100 ms in the presence of CO_2 seeded at 0.5% in the helium-trapping gas. Major fragments correspond to $(6,n,2k)^{1-}$ species similar to what is observed with O_2 traces. No CO_2 adduct peak is directly identified. However, some mis-shaped minor peaks are observed at m/z 999.8 and 1110.1 about 42 Th above ions $(6,3,7)^{1-}$ and $(6,2,8)^{1-}$. Under the assumption that the peak fronting is associated with the detection of metastable ions, it is likely that these peaks correspond to fragile CO_2 adducts detected at lower *m/z* due to dissociation during detection. **26**

 This journal is © The Royal Society of Chemistry 20xx

Please do not adjust margins

Complements

S1 - Collision rate calculation details:

The collision rate (k_{coll}) between an ion and the neutral reagents introduced in the ion trap is the product of the neutral capture rate coefficient of the ion ($k_{capture}$) by the number density of neutrals ($N_{density}$).

The number density of neutrals in the ion trap is estimated from the ion trap pressure documented in the literature: 5e-3 Torrs in the high-pressure trap and 4e-4 Torrs in the low-pressure trap.[1] It is then balanced by the seeding percentage of the reagent of interest. For O_2/CO_2 introduced at 5000 ppm in helium: N^{HPT} = 8.1e11 cm^{-3}; N^{LPT} = 6.5e10 cm^{-3}

Capture rate coefficients are calculated with the programme Colrate[2] with the following parameters:

- Temperature 300 K
- For neutrals:
  - For O_2: polarizability (1.562 Å3) ; dipole (0 D); mass (32 amu); moment of inertia (11.72561 amu.Å2)
  - For CO_2: polarizability (2.507 Å3); dipole (0 D); mass (44 amu); moment of inertia (43.2 amu.Å2)
- For ions:
  - $(6,14,0)^{2-}$: mass (2350 amu); charge -2
  - $(6,14,0)^{1-}$: mass (2350 amu); charge -1
  - $(6,13,0)^{2-}$: mass (2224 amu); charge -2
  - $(6,13,0)^{1-}$: mass (2224 amu); charge -1
  - $(6,12,0)^{1-}$: mass (2097 amu); charge -1

$k_{capture}$ (molecule.cm^3.s^{-1})	$(6,14,0)^{2-}$	$(6,13,0)^{1-}$	$(6,13,0)^{2-}$	$(6,13,0)^{1-}$	$(6,12,0)^{1-}$
O_2	1.0379 e-9	0.5188 e-9	1.0383 e-9	0.5192 e-9	0.5194 e-9
CO_2	1.1238 e-9	0.5619 e-9	1.1244 e-9	0.5622 e-9	0.5625 e-9

As a result,

- $k_{coll}^{HPT}(O_2,(6,14,0)^{2-})$ = 8.1e11 x 1.0379e-9 = 840 s^{-1};
- $k_{coll}^{LPT}(O_2,(6,14,0)^{2-})$ = 6.5e10 x 1.0379e-9 = 67 s^{-1};
- $k_{coll}^{HPT}(CO_2,(6,14,0)^{2-})$ = 8.1e11 x 1.1238e-9 = 910 s^{-1};
- $k_{coll}^{LPT}(CO_2,(6,14,0)^{2-})$ = 6.5e10 x 1.1238e-9 = 73 s^{-1};

References:

[1] T. P. Second, J. D. Blethrow, J. C. Schwartz, G. E. Merrihew, M. J. MacCoss, D. L. Swaney, J. D. Russell, J. J. Coon and V. Zabrouskov, Dual-pressure linear ion trap mass spectrometer improving the analysis of complex protein mixtures, Anal. Chem., 2009, 81, 7757–7765.

[2] K. F. Lim, COLRATE. QCPE 643: Calculation of gas-kinetic collision rate coefficients, Quantum Chem. Progr. Exch. Bull.

S2 - Secondary fragments: full description and discussion of the $(6,n,0)^{1-}$ series

In addition to the three primary photo-fragment ions discussed above, several ion series are observed in the LID mass spectrum (see Figure 6 and Scheme 1). The first series corresponds to iodine depleted cluster complexes from $(6,12,0)^{1-}$ to $(6,7,0)^{1-}$. They may arise as secondary fragments from sequential losses of I_2 (Scheme 1, black arrows) from either primary fragments $(6,14,0)^{1-\bullet}$ or $(6,13,0)^{1-}$, as suggested by the alternating intensity pattern. Indeed, $(6,n,0)^{1-}$ species form two separate ion series with a constantly decreasing intensity trend for n = 14, 12, 10, 8 on the one hand, *i.e.* from the low-intensity species $(6,14,0)^{1-\bullet}$, and, on the other hand for n = 13, 11, 9, 7, *i.e.* from the high intensity species $(6,13,0)^{1-}$ (see Figure 6). Interestingly, no I_2 loss is observed by low energy resonant CID activation of $(6,14,0)^{1-\bullet}$ (or higher energy resonant CID for $(6,13,0)^{1-}$, see Figure S5). This indicates that the I_2 loss is less favoured than the barrierless $I^\bullet$ loss. However, I_2 loss is likely thermodynamically favoured compared to 2 losses

Please do not adjust margins

of $I^{\bullet}$, due to the ~1.54 eV I_2 bond stabilization.[1] It may explain why in the case of UV photodissociation at 260 nm (Figure 6), where 4.77 eV is provided at once, I_2 losses are observed rather than sequential $I^{\bullet}$ losses. Since I_2 losses may require substantial ligand rearrangement with possibly high kinetic barrier, it is also possible that the successive I_2 losses observed experimentally arise from dissociation in the electronic excited states rather than from vibrationally excited (hot) ground state. Lastly, the intensity of the first I_2 loss fragments, $(6,12,0)^{1-}$ and $(6,11,0)^{1-}$, are respectively 0.15 and 0.8 relative to their respective monoanionic primary fragments $(6,14,0)^{1-\bullet}$ and $(6,13,0)^{1-}$ (see Figure 6). It shows that I_2 loss from $(6,14,0)^{1\bullet-}$ is less favoured: under the hypothesis that the barrier to I_2 loss is identical for both precursors, this may indicate that there is more internal energy available in the cluster after the loss of I^- than after the detachment of one electron, consistent with the higher photon energy threshold observed for photo-detachment than photo-dissociation (see Figure 4).

Alternatively, the $(6,n,0)^{1-}$ species may arise from consecutive $I^{\bullet}$ losses (Scheme 1, red arrows). Indeed, Figures S1 and S2 respectively show that both $(6,14,0)^{1-\bullet}$ and $(6,13,0)^{1-}$ lose $I^{\bullet}$ upon CID activation. Figure S1 additionally shows that although the collisional energy is low (NCE = 6), the fragmentation efficiency of the oxidized cluster $(6,14,0)^{1-\bullet}$ is very high (precursor survival yield ~2%), indicative of its instability. This suggests that part of the $(6,13,0)^{1-}$ population in Figure 1 may come from the decay of $(6,14,0)^{1-\bullet}$, accelerated by the residual energy post electron detachment at 260 nm. In the case of $(6,13,0)^{2-\bullet}$, the highly predominant fragment is I^- loss (Figure S3), which brings back to the mono-anionic series $(6,n,0)^{1-}$. Also, even at a remarkably low collisional energy (NCE = 2), the $(6,13,0)^{2-\bullet}$ survival yield is low (4 %), which is indicative of its high instability and susceptibility to fragment as well as to react with O_2 (see section "Reactivity of the photofragments with O_2" in Manuscript). Indeed, the calculated Gibbs free energy of the addition reaction of O_2 to $(6,13,0)^{2-\bullet}$ reveal that it is significantly exergonic (-1.221 eV). Thus, iodide loss from the dianion may be an alternative, low energy formation path for $(6,12,0)^{1-}$ in Figure 6 that does not require the oxidized species $(6,14,0)^{1-}$. In general, iodine loss would be consistent with prior mass spectrometry results by Warneke et al[2] which revealed that upon collisional activation and after the initial loss of iodide I^-, further losses of halogen radicals represent the main fragmentation channels.

QC geometry optimizations were performed to yield the relaxed geometries and energies of the $(6,n,0)^{1-}$ species generated from sequential $I^{\bullet}$ losses starting from $(6,13,0)^{1-}$ (more details in Table S3 header). The Gibbs free energy changes ($\Delta G^{298\ K}$) associated with each successive $I^{\bullet}$ loss reactions are given in Table S4 for $(6,n,0)^{1-}$ parents from n = 14 down to n = 6, and the associated parent/product structures are represented from n = 12 to n = 7 in Figure 7 left column. All $I^{\bullet}$ loss reactions are endergonic and range from +3.877 eV for parent $(6,7,0)^{1-}$ to +2.794 eV for parent $(6,10,0)^{1-}$. Whereas the first two iodine atoms are more favourably removed from apical sites, it becomes less endergonic to remove an inner iodine from $(6,12,0)^{1-}$, consistent with simulation results of Warneke and coworkers.[2] Then, three more apical iodine atoms may be removed to yield $(6,8,0)^{1-}$ from which a second inner iodine is again removed to yield the most stable $(6,7,0)^{1-}$ with 2 free inner coordination sites (see Figure 7).

In any case, whether it results from I_2 or from $I^{\bullet}$ losses, the formation of such secondary fragments is energy demanding and requires excess energy in the primary fragments. It could also result from the absorption of secondary photons by the primary fragments, although this alternative is less probable due to the short timescale of the nanosecond laser pulse. Lastly, these secondary fragments could result from the reaction of primary fragments with neutral reagent traces in the helium background gas (see section "Reactivity of the photofragments with O_2" in Manuscript).

Interestingly, Warneke and coworkers have shown with ion mobility and computational simulations that the octahedral Mo_6 structure remains largely unchanged in the iodine-depleted Mo_6 complexes.[2] This is consistent with prior ion mobility mass spectrometry results in our group which showed that the Mo_6 cluster size and shape are retained irrespective of the chemical nature of the ligands (halogenides or hydroxides),[3] which advocates for a very robust Mo_6 octahedral cluster structure. It is also what we calculate for the series $(6,n,0)^{1-}$ for n ranging from 14 to 5. It should nevertheless be emphasized that the symmetry of the Mo_6 core is importantly decreased. Indeed, in order to compensate for the electronic depletion due to the iodine departure, the metal-metal bonds involving the more I-depleted Mo atoms are importantly shortened: down to 2.391 Å in $(6,5,0)^{1-}$, compared to 2.678 Å in the parent $(6,14,0)^{2-}$ cluster. The shorter Mo-Mo distance in I-depleted sites is in the order of magnitude of reported triple Mo-Mo bonds (while close to bond order 1 in the parent cluster).[4]

[1] R. F. Barrow, D. F. Broyd, L. B. Pederson and K. K. Yee, The dissociation energies of gaseous Br2 and I2, Chem. Phys. Lett., 1973, 18, 357–358.

[2] P. Su, Z. Warneke, D. Volke, M. F. Espenship, H. Hu, S. Kawa, K. Kirakci, R. Hoffmann, J. Laskin, C. Wiebeler and J. Warneke, Gas Phase Reactivity of [Mo 6 X 14] 2– Dianions (X = Cl – I), J. Am. Soc. Mass Spectrom., 2023, 34, 161–170.

[3] K. Harada, T. K. N. Nguyen, F. Grasset, C. Comby-Zerbino, L. MacAleese, F. Chirot, P. Dugourd, N. Dumait, S. Cordier, N. Ohashi, M. Matsuda and T. Uchikoshi, Light-dependent ionic-electronic conduction in an amorphous octahedral molybdenum cluster thin film, NPG Asia Mater., 2022, 14, 21.

[4] M. H. Chisholm, Metal-metal bonds and metal-carbon bonds in the chemistry of molybdenum and tungsten alkoxides, Polyhedron, 1983, 2, 681–722.

 This journal is © The Royal Society of Chemistry 20xx

Please do not adjust margins

Please do not adjust margins

S3 – Details on the experimental optical spectroscopy method

For spectroscopy, the optical action (fragmentation) spectrum of $[Mo_6I_{14}]^{2-}$ was measured by irradiating the mass selected precursors with a single laser pulse from a UV-Vis optical parametric oscillator (Horizon OPO pumped at 10 Hz with the third harmonic of Surelite-I Nd:YAG laser, Continuum, Amplitude Laser Inc.). The OPO was scanned by 2 nm pitches, over the 3 following wavelength ranges: 200-290 nm, 290-390 nm and 410-600 nm. For each range, the laser was realigned (at 260, 340 and 540 nm respectively) and the laser power adjusted to ensure that the fragmentation ratio remains below 1% at the optimization wavelength. Two hundred single mass spectra were recorded for each wavelength. In order to allow for a single laser pulse to interact with trapped ions, the OPO pump was externally triggered using a delay generator (DG645, Stanford Research Systems) and a mechanical shutter (SH05/TSC001, Thorlabs) was open only for one full DG645 cycle during the ion activation time (130 ms). An Arduino Uno microcontroller performs the simple logic required to actuate the shutter upon reception of trigger signals from both the ion trap and the DG645.

In order to generate optical fragmentation spectra, ion intensities (see Table S0) are extracted and the precursor fragmentation ratio is calculated from each individual mass spectrum. These fragmentation ratios are grouped per wavelength and statistically analysed (median, mean, quartile positions, etc.). The medians are then used and after baseline correction and smoothing, they are divided by a factor proportional to the generic laser profile (power*wavelength) in order to account for fluctuations of the number of photons along the wavelength range. The result is called fragmentation yield. This data analysis is performed independently on each wavelength range of acquisition (see Figure S0). Inter-range relative intensities are meaningless and may be scaled to facilitate interpretation.

For the chemical study of $[Mo_6I_{13}]^-$, $[Mo_6I_{13}]^{2-\bullet}$ and $[Mo_6I_{14}]^{-\bullet}$ species, precursor ions $[Mo_6I_{14}]^{2-}$ were mass selected and irradiated during the MS^2 stage with a single, 1 mJ, 5 nanosecond OPO pulse at the set wavelength 260 nm. The resulting $[Mo_6I_{13}]^-$, $[Mo_6I_{13}]^{2-\bullet}$ or $[Mo_6I_{14}]^{-\bullet}$ ions were then isolated and allowed to relax and/or react with the background trapping gas during the MS^3 stage. In order to probe the reactivity of $[Mo_6I_{13}]^-$ and $[Mo_6I_{13}]^{2-\bullet}$ species as well as other selected ions, the trapping helium buffer gas was seeded with O_2 or CO_2 at 5000 ppm (respectively 840/67 and 910/73 collisions per second with trapped Mo_6 di-/mono-anions. Estimations from Colrate, see SI Complements S1). Reaction times, varied by using the MS^3 ion "activation time" with no collisional energy, were explored up to 10 s before MS acquisition.

For photochemical investigations, precursor ions $[Mo_6I_9]^-$ were mass selected and trapped during variable reaction times in the presence of CO_2 in a similar MS^3 sequence as above, but with the addition of constant irradiation with a 488 nm CW laser set at 80 mW.

Assignment for fragment ions in Figures 1, 6 and 11 are detailed in Supporting Information Tables S1 and S2.

S4 – Details on the COSMO correction

The incompleteness of the atomic basis sets and the self-interaction error inherent in DFT is responsible (in some cases) for the energy of the highest occupied molecular orbital (HOMO) to become positive. This is particularly true for heavily-charged anions. Positive HOMO levels correspond to continuum orbital with no physical meaning and lead to erroneous calculations. In order to circumvent this issue, basis set are enlarged to the maximum (quadruple-zeta slater functions). However, if it is insufficient, a moderate external effect can be applied by the conductor–like screening model (COSMO) that could be interpreted as simulating the gas phase environment. The dielectric constant chosen (1.45) globally shift downwards the energies of the molecular orbitals and does not induce any additional polarization (no modification of the energy difference nor of the spatial extension of orbitals - this was tested). This COSMO correction was applied to all systems irrelevant of their charge for all calculation types (optimization of geometry, TD-DFT…). These precisions are now added to the computational details.

Please do not adjust margins

Tables

Table S0 - Peak list and integration windows for the analysis of $[Mo_6I_{14}]^{2-}$ action spectra in Figures 2 & 3.

#	Assignment	[low bound, high bound]
1	(6,14)2-	[1175., 1177.05]
2	(6,13)2-	[1110., 1115.]
3	(6,13,2)2-	[1126., 1131.]
4	(6,14)1-	[2350., 2354.]
5	(6,13)1-	[2224., 2227.4]
6	(6,12)1-	[2097., 2100.5]
7	(6,12,2)1-	[2129., 2132.5]
8	(6,11)1-	[1970., 1973.5]
9	(6,11,2)1-	[2002., 2005.5]
10	(6,10)1-	[1843., 1846.5]
11	(6,9)1-	[1716., 1720.]
12	(6,9,2)1-	[1748., 1752.]
13	(6,9,4)1-	[1780., 1784.]
14	(6,8)1-	[1589., 1593.]
15	(6,8,2)1-	[1621., 1625.]
16	(6,8,4)1-	[1653., 1657.]
17	(6,7,2)1-	[1494., 1498.]
18	(6,7,4)1-	[1526., 1530.]
19	(6,6,2)1-	[1367., 1371.]
20	(6,6,4)1-	[1399., 1403.]
21	(6,6,6)1-	[1431., 1435.]
22	(6,5,4)1-	[1272., 1276.]
23	(6,5,6)1-	[1304., 1308.]
24	(6,4,6)1-	[1177.6, 1179.6]
25	(5,11)1- & (6,10,2)1-	[1870., 1882.]
26	(1,2,2)1-	[376., 390.].

Table S1 - Peak list, mass differences and assignments for MS in Figures 1 and 6.

m/z (observed)	*z*	Relative intensity	Assignment	*m/z (assignment)*	*Δm/z (obs. – assign.)*
1175.18	2	1.E+00	(6,14,0)2-	1175.18	-
2350.55	1	3.E-01	(6,14,0)1-	2350.36	0.19
2223.73	1	1.E+00	(6,13,0)1-	2223.46	0.27
2128.82	1	6.E-03	(6,12,2)1-	2128.54	0.28
2096.91	1	5.E-02	(6,12,0)1-	2096.55	0.36
1970	1	8.E-01	(6,11,0)1-	1969.65	0.35
1875.18	1	3.E-03	(6,10,2)1-	1874.73	0.45
1843.18	1	4.E-02	(6,10,0)1-	1842.74	0.44
1748.36	1	2.E-01	(6,9,2)1-	1747.83	0.53
1716.36	1	3.E-01	(6,9,0)1-	1715.84	0.52
1653.55	1	5.E-02	(6,8,4)1-	1652.91	0.64
1621.55	1	4.E-02	(6,8,2)1-	1620.92	0.63

This journal is © The Royal Society of Chemistry 20xx

1589.55	1	1.E-02	(6,8,0)1-	1588.93	0.62
1526.64	1	3.E-02	(6,7,4)1-	1526.01	0.63
1494.64	1	1.E-02	(6,7,2)1-	1494.02	0.62
1462.73	1	3.E-03	(6,7,0)1-	1462.03	0.70
1431.73	1	5.E-03	(6,6,6)1-	1431.09	0.64
1399.82	1	1.E-02	(6,6,4)1-	1399.10	0.72
1367.73	1	1.E-03	(6,6,2)1-	1367.11	0.62
1335.91	1	2.E-04	(6,6,0)1-	1335.12	0.79
1305	1	1.E-02	(6,5,6)1-	1304.19	0.81
1272.91	1	5.E-03	(6,5,4)1-	1272.20	0.71
1240	1	2.E-04	(6,5,2)1-	1240.21	-0.21
1209.06	1	1.E-05	(6,5,0)1-	1208.22	0.84
1111.82	2	2.E-02	(6,13,0)2-	2223.46	0.09

Table S2 - Peak list, mass differences and assignments for MS in Figure 11.

m/z (observed)	*z*	Relative intensity	Assignment	*m/z (assignment)*	*Δm/z (obs. – assign.)*
1716.45	1	1.E+00	(6,9,0)1-	1716.45	-
1589.64	1	1.7E-01	(6,8,0)1-	1589.55	0.09
1605.6	1	6.0E-03	(6,8,1)1-	1605.54	0.06
1621.55	1	1.0E-02	(6,8,2)1-	1621.54	0.01
1462.74	1	4.0E-02	(6,7,0)1-	1462.64	0.10
1478.73	1	2.0E-02	(6,7,1)1-	1478.64	0.09
1494.73	1	1.2E-01	(6,7,2)1-	1494.63	0.10
1367.92	1	8.0E-03	(6,6,2)1-	1367.73	0.19
1383.88	1	5.0E-03	(6,6,3)1-	1383.72	0.16
1399.88	1	3.0E-02	(6,6,4)1-	1399.72	0.16
1241.06	1	4.0E-03	(6,5,2)1-	1240.82	0.24
1257.18	1	5.0E-04	(6,5,3)1-	1256.82	0.36
1273.06	1	6.8E-02	(6,5,4)1-	1272.81	0.25
1289.06	1	4.0E-03	(6,5,5)1-	1288.81	0.25
1305.06	1	3.2E-02	(6,5,6)1-	1304.80	0.26
1130.24	1	4.0E-03	(6,4,3)1-	1129.91	0.33
1146.36	1	4.0E-03	(6,4,4)1-	1145.91	0.45
1162.28	1	4.0E-03	(6,4,5)1-	1161.90	0.38
1178.27	1	1.55E-01	(6,4,6)1-	1177.90	0.37
1051.45	1	2.6E-01	(6,3,6)1-	1050.99	0.46

This journal is © The Royal Society of Chemistry 20xx

Please do not adjust margins

1067.45	1	2.6E-02	(6,3,7)1-	1066.99	0.46
924.61	1	2.0E-02	(6,2,6)1-	924.09	0.52
940.62	1	2.0E-02	(6,2,7)1-	940.08	0.54
956.62	1	4.5E-02	(6,2,8)1-	956.08	0.54
829.82	1	1.2E-02	(6,1,8)1-	829.17	0.65
845.8	1	2.0E-03	(6,1,9)1-	845.17	0.63
861.73	1	1.2E-02	(6,1,10)1-	861.16	0.57
734.91	1	2.0E-02	(6,0,10)1-	734.26	0.65
750.91	1	4.0E-03	(6,0,11)1-	750.25	0.66
766.91	1	2.0E-02	(6,0,12)1-	766.25	0.66

Table S3 - SCM-ADF energies ($E_{SCM-ADF}$), Gibbs free energies ($G_{SCM-ADF}$) and enthalpies ($H_{SCM-ADF}$) at 298 K of all ions and molecules calculated.

SCM-ADF energies ($E_{SCM-ADF}$), Gibbs free energies ($G_{SCM-ADF}$) and enthalpies ($H_{SCM-ADF}$) at 298 K of all ions and molecules which geometries were optimized: CO, CO_2, I, I^-, I_2, O_2, $[Mo_6I_{14}]^{2-}$, $[Mo_6I_n]^{1-}$ for *n* = 14-5, $[Mo_6I_nO_2]^{1-}$ for *n* = 14-6. The spin state and isomer ordering are indicated. The SCM-ADF energy corresponds to the binding energy between bare nuclei and free electrons, see https://www.scm.com/doc/ADF/Input/Bond_energy_analysis.html. The Cartesian coordinates are available at https://doi.org/10.5281/zenodo.15519713. The $[Mo_6I_n]^-$ geometries were obtained by a sequential procedure which consists in calculating the removal of each possible $I^\bullet$ loss position and keeping the most stable isomer as starting geometry for the subsequent $I^\bullet$ loss, starting from the optimized $[Mo_6I_{13}]^-$. The singlet and triplet states or doublet and quartet states have been calculated (accordingly with the electronic structure of the system). Additionally, I-apical-only cleavages were also considered for each $[Mo_6I_n]^{1-}$. Starting from n = 11, they are not the most stable structures. The $[Mo_6I_nO_2]^-$ were obtained by coordinating an O_2 molecule to each possible Mo atoms using the most stable $[Mo_6I_n]^-$ geometries (isomer), or by removing $I^\bullet$ to $[Mo_6I_{n+1}O_2]^-$ most stable geometry (all $I^\bullet$ position tested) (isomerb). The singlet and triplet states or doublet and quartet states have been calculated (accordingly with the electronic structure of the system).

Compound *spin state* isomer(b) order	$E_{SCM-ADF}$ (eV)	$G_{SCM-ADF}$ (eV)	$H_{SCM-ADF}$ (eV)	Reference to access to the Cartesian coordinates in the text file available at: https://doi.org/10.5281/zenodo.15519713
CO *singlet*	-14.670	-15.060	-14.449	./CO/CO.run.202909.log
CO_2 *singlet*	-22.738	-23.104	-22.323	./CO2/CO2.run.202353.log
I *doublet*	-0.252	-0.252	-0.252	./I/I-neutre.run.182258.log
I^{1-} *singlet*	-4.153	-4.153	-4.153	./Imoins/I-moins.run.182259.log
I_2 *singlet*	-2.586	-2.468	-3.274	./I2.run.204526.logfile
O_2 *triplet*	-9.792	-10.213	-9.607	./O2/O2-trip.run.201933.log
$[Mo_6I_{14}]^{2-}$ *singlet*	-102.139	-103.992	-100.582	./I14-2moins/Mo6I14-2moins-solv-N2.run.164228.log
$[Mo_6I_{14}]^{1-}$ *doublet*	-99.436	-101.237	-97.935	./I14-1moins/Mo6I14-1moins-solv-N2-opt.run.198236.log
$[Mo_6I_{13}]^{2-}$ *doublet*	-98.396	-100.199	-96.921	./I13-2moins/Mo6I13-2moins-solv-N2.run.164233.log

This journal is © The Royal Society of Chemistry 20xx

Please do not adjust margins

Please do not adjust margins

$[Mo_6I_{13}O_2]^{2-}$ *doublet* isomer 1	-109.882	-111.632	-108.200	./I13O2-2moins/Mo6I13O2-2moins-solv-N2.run.181874.log
$[Mo_6I_{13}O_2]^{2-}$ *doublet* isomer 2	-109.789	-108.101	-111.547	./I13O2-2moins/Mo6I13O2-inner-2moins-solv-N2.run.181873.log
$[Mo_6I_{13}O_2]^{2-}$ *quartet* isomer 1	-108.521	-110.328	-106.848	./I13O2-2moins/Mo6I13O2-2moins-quar-solv-N2.run.207451.log
$[Mo_6I_{13}]^{1-}$ *singlet*	-97.251	-98.996	-95.771	./I13-1moins/Mo6I13-1moins-solv-N2.run.164230.log
$[Mo_6I_{13}]^{1-}$ *triplet*	-95.953	-97.761	-94.480	./I13-1moins/Mo6I13-1moins-solv-N2-triplet.run.172132.logfile
$[Mo_6I_{13}O_2]^{1-}$ *triplet* isomer 1	-107.539	-109.235	-105.908	./I13O2-1moins/Mo6I13O2-1moins-trip-solv-N2-opt.run.201988.log
$[Mo_6I_{13}O_2]^{1-}$ *singlet* isomer 1	-107.435	-109.126	-105.743	./I13O2-1moins/Mo6I13O2-1moins-sing-solv-N2-opt.run.202403.log
$[Mo_6I_{12}]^{1-}$ *doublet* isomer 1	-94.019	-95.703	-92.621	./I12-1moins/Mo6I12-trans-1moins-doub-solv-N2-opt.run.197970.log
$[Mo_6I_{12}]^{1-}$ *doublet* isomer 2	-93.729	-95.414	-92.331	./I12-1moins/Mo6I12-adja-1moins-doub-solv-N2-opt.run.197964.log
$[Mo_6I_{12}]^{1-}$ *doublet* isomer 3	-93.541	-95.190	-92.196	./I12-1moins/Mo6I12-innertrans-1moins-doub-solv-N2-opt.run.197967.log
$[Mo_6I_{12}]^{1-}$ *doublet* isomer 4	-93.319	-94.985	-91.947	./I12-1moins/Mo6I12-inneradj-1moins-doub-solv-N2-opt.run.198222.logfile
$[Mo_6I_{12}]^{1-}$ *quartet* isomer 1	-92.317	-94.077	-90.925	./I12-1moins/Mo6I12-adja-1moins-quar-solv-N2-opt.run.198221.log
$[Mo_6I_{12}]^{1-}$ *quartet* isomer 2	-92.275	-94.063	-90.912	./I12-1moins/Mo6I12-innertrans-1moins-quar-solv-N2-opt.run.202381.log
$[Mo_6I_{12}]^{1-}$ *quartet* isomer 3	-92.220	-93.969	-90.827	./I12-1moins/Mo6I12-trans-1moins-quar-solv-N2-opt.run.198223.log
$[Mo_6I_{12}]^{1-}$ *quartet* isomer 4	-91.959	-93.748	-90.596	./I12-1moins/Mo6I12-inneradj-1moins-quar-solv-N2-opt.run.202380.log
$[Mo_6I_{12}O_2]^{1-}$ *doublet* isomer 1	-105.181	-106.812	-103.571	./I12O2-1moins/Mo6I12O2-trans-1moins-doub-solv-N2-opt.run.200605.log
$[Mo_6I_{12}O_2]^{1-}$ *quartet* isomer 1	-103.995	-105.714	-102.392	./Mo6I12O2-trans-1moins-quar-solv-N2-opt.run.204396.log
$[Mo_6I_{11}]^{1-}$ *singlet* isomer 1	-90.739	-92.398	-89.420	./I11-1moins/Mo6I11-inner-1moins-sing-solv-N2-opt.run.198247.log
$[Mo_6I_{11}]^{1-}$ *triplet* isomer 1	-90.368	-91.993	-89.051	./I11-1moins/Mo6I11-api-1moins-trip-solv-N2-opt.run.198991.log
$[Mo_6I_{11}]^{1-}$ *singlet* isomer 2	-90.251	-91.895	-88.935	./I11-1moins/Mo6I11-api-1moins-sing-solv-N2-opt.run.198246.log
$[Mo_6I_{11}]^{1-}$ *triplet* isomer 2	-89.977	-91.551	-88.713	./I11-1moins/Mo6I11-inner-1moins-trip-solv-N2-opt.run.198897.log
$[Mo_6I_{11}O_2]^{1-}$ *singlet* isomer 1, O-O clivage	-105.780	-107.361	-104.240	./I11O2-1moins/Mo6I11O2-1moins-sing-inner-vac-inner-solv-N2-opt.run.201361.log
$[Mo_6I_{11}O_2]^{1-}$ *singlet* isomer 2, O-O clivage	-105.779	-107.361	-104.240	./I11O2-1moins/Mo6I11O2-1moins-sing-inner-trans-solv-N2-opt.run.201231.log
$[Mo_6I_{11}O_2]^{1-}$ *singlet* isomer 3, O-O clivage	-105.779	-107.361	-104.240	./I11O2-1moins/Mo6I11O2-1moins-singl-inner-vactriangle-solv-N2-opt.run.199232.log
$[Mo_6I_{11}O_2]^{1-}$ *triplet* isomer 1, O-O clivage	-105.347	-106.934	-103.814	./I11O2-1moins/Mo6I11O2-1moins-trip-inner-vactriangle-solv-N2-opt.run.199229.log
$[Mo_6I_{11}O_2]^{1-}$ *triplet* isomer 2	-102.182	-103.722	-100.680	./I11O2-1moins/Mo6I11O2-1moins-trip-inner-trans-solv-N2-opt.run.199231.log
$[Mo_6I_{11}O_2]^{1-}$ *triplet* isomer 3	-102.182	-103.722	-100.680	./I11O2-1moins/Mo6I11O2-1moins-trip-inner-vac-inner-solv-N2-opt.run.199863.log
$[Mo_6I_{11}O_2]^{1-}$ *triplet* isomerb 1	-102.182	-103.721	-100.679	./Mo6I12O2-mI15-1moins-trip-solv-N2-opt.run.204133.log

Please do not adjust margins

Please do not adjust margins

$[Mo_6I_{11}O_2]^{1-}$ *singlet* isomerb 1	-101.773	-103.347	-100.250	./Mo6I12O2-mI8-1moins-sing-solv-N2-opt.run.202215.log
$[Mo_6I_{11}O_2]^{1-}$ *singlet* isomerb 2	-101.747	-103.315	-100.224	./Mo6I12O2-mI11-1moins-sing-solv-N2-opt.run.202218.log
$[Mo_6I_{11}O_2]^{1-}$ *singlet* isomerb 3	-101.747	-103.315	-100.224	./Mo6I12O2-mI13-1moins-sing-solv-N2-opt.run.202352.log
$[Mo_6I_{11}O_2]^{1-}$ *singlet* isomerb 4	-101.747	-103.314	-100.223	./Mo6I12O2-mI9-1moins-sing-solv-N2-opt.run.202216.log
$[Mo_6I_{11}O_2]^{1-}$ *singlet* isomerb 5	-101.746	-103.314	-100.223	./Mo6I12O2-mI10-1moins-sing-solv-N2-opt.run.202940.log
$[Mo_6I_{11}O_2]^{1-}$ *singlet* isomerb 6	-101.723	-103.310	-100.194	./Mo6I12O2-mI7-1moins-sing-solv-N2-opt.run.202221.log
$[Mo_6I_{11}O_2]^{1-}$ *triplet* isomerb 2	-101.676	-103.251	-100.148	./Mo6I12O2-mI8-1moins-trip-solv-N2-opt.run.202974.log
$[Mo_6I_{11}O_2]^{1-}$ *triplet* isomerb 3	-101.674	-103.251	-100.147	./Mo6I12O2-mI9-1moins-trip-solv-N2-opt.run.202975.log
$[Mo_6I_{11}O_2]^{1-}$ *triplet* isomerb 4	-101.674	-103.251	-100.146	./Mo6I12O2-mI10-1moins-trip-solv-N2-opt.run.202585.log
$[Mo_6I_{11}O_2]^{1-}$ *triplet* isomerb 5	-101.665	-103.248	-100.138	./Mo6I12O2-mI7-1moins-trip-solv-N2-opt.run.202973.log
$[Mo_6I_{11}O_2]^{1-}$ *singlet* isomerb 7	-101.556	-103.118	-100.052	./Mo6I12O2-mI12-1moins-sing-solv-N2-opt.run.202219.log
$[Mo_6I_{11}O_2]^{1-}$ *singlet* isomerb 8	-101.556	-103.118	-100.051	./Mo6I12O2-mI15-1moins-sing-solv-N2-opt.run.202597.log
$[Mo_6I_{11}O_2]^{1-}$ *triplet* isomerb 6	-101.473	-103.029	-99.996	./Mo6I12O2-mI12-1moins-trip-solv-N2-opt.run.205092.log
$[Mo_6I_{11}O_2]^{1-}$ *triplet* isomerb 7	-101.318	-102.903	-99.818	./Mo6I12O2-mI13-1moins-trip-solv-N2-opt.run.204132.log
$[Mo_6I_{11}O_2]^{1-}$ *triplet* isomerb 8	-101.313	-102.910	-99.813	./Mo6I12O2-mI11-1moins-trip-solv-N2-opt.run.203371.log
$[Mo_6I_{10}]^{1-}$ *doublet* isomer 1	-87.295	-88.900	-86.058	./I10-1moins/Mo6I10-1moins-doub-7-solv-N2-opt.run.199970.log
$[Mo_6I_{10}]^{1-}$ *doublet* isomer 2	-87.171	-88.759	-85.933	./I10-1moins/Mo6I10-1moins-doub-8-solv-N2-opt.run.199971.log
$[Mo_6I_{10}]^{1-}$ *doublet* isomer 3	-86.907	-88.580	-85.671	./I10-1moins/Mo6I10-1moins-doub-12-solv-N2-opt.run.199973.log
$[Mo_6I_{10}]^{1-}$ *doublet* isomer 4	-86.878	-88.536	-85.642	./I10-1moins/Mo6I10-1moins-doub-13-solv-N2-opt.run.199972.log
$[Mo_6I_{10}]^{1-}$ *doublet* isomer 5	-86.793	-88.398	-85.559	./I10-1moins/Mo6I10-1moins-doub-full-inner-api-syn-solv-N2-opt.run.201807.log
$[Mo_6I_{10}]^{1-}$ *doublet* isomer 6	-86.729	-88.336	-85.519	./I10-1moins/Mo6I10-1moins-doub-11-solv-N2-opt.run.200653.log
$[Mo_6I_{10}]^{1-}$ *quartet* isomer 1	-86.661	-88.212	-85.425	./Mo6I10-1moins-quar-full-inner-api-syn-solv-N2-opt.run.214902.log
$[Mo_6I_{10}]^{1-}$ *quartet* isomer 2	-86.652	-88.215	-85.416	./Mo6I10-1moins-quar-full-inner-api-trans-solv-N2-opt.run.214903.log
$[Mo_6I_{10}]^{1-}$ *doublet* isomer 7	-86.617	-88.207	-85.383	./I10-1moins/Mo6I10-1moins-doub-full-inner-api-trans-solv-N2-opt.run.201808.log
$[Mo_6I_{10}]^{1-}$ *quartet* isomer 3	-86.499	-88.118	-85.294	./Mo6I10-1moins-quar-7-solv-N2-opt.run.214899.log
$[Mo_6I_{10}]^{1-}$ *quartet* isomer 4	-86.060	-87.624	-84.852	./Mo6I10-1moins-quar-8-solv-N2-opt.run.214901.log
$[Mo_6I_{10}]^{1-}$ *quartet* isomer 5	-85.974	-87.440	-84.843	./Mo6I10-1moins-quar-12-solv-N2-opt.run.214897.log
$[Mo_6I_{10}]^{1-}$ *quartet* isomer 6	-85.932	-87.563	-84.724	./Mo6I10-1moins-quar-13-solv-N2-opt.run.214898.log
$[Mo_6I_{10}]^{1-}$ *quartet* isomer 7	-85.716	-87.314	-84.537	./Mo6I10-1moins-quar-11-solv-N2-opt.run.214896.log
$[Mo_6I_{10}O_2]^{1-}$ *doublet* isomerb 1, O-O clivage	-102.886	-104.431	-101.432	./I11O2-1moins/Mo6I11O2-mI12-1moins-doub-solv-N2-opt.run.202229.log
$[Mo_6I_{10}O_2]^{1-}$ *doublet* isomerb 2, O-O clivage	-102.809	-104.317	-101.354	./I11O2-1moins/Mo6I11O2-mI7-1moins-doub-solv-N2-opt.run.202385.log

This journal is © The Royal Society of Chemistry 20xx

Please do not adjust margins

$[Mo_6I_{10}O_2]^{1-}$ *doublet* isomerb 3, O-O clivage	-102.780	-104.274	-101.327	./I11O2-1moins/Mo6I11O2-mI8-1moins-doub-solv-N2-opt.run.202384.log
$[Mo_6I_{10}O_2]^{1-}$ *doublet* isomerb 4, O-O clivage	-102.724	-104.215	-101.294	./I11O2-1moins/Mo6I11O2-mI14-1moins-doub-solv-N2-opt.run.204137.log
$[Mo_6I_{10}O_2]^{1-}$ *quartet* isomerb 1, O-O clivage	-102.345	-103.853	-100.918	./Mo6I11O2-mI14-1moins-quar-solv-N2-opt.run.204358.log
$[Mo_6I_{10}O_2]^{1-}$ *doublet* isomerb 5, O-O clivage	-102.327	-103.863	-100.872	./I11O2-1moins/Mo6I11O2-mI11-1moins-doub-solv-N2-opt.run.202228.log
$[Mo_6I_{10}O_2]^{1-}$ *quartet* isomerb 2, O-O clivage	-102.318	-103.818	-100.890	./Mo6I11O2-mI12-1moins-quar-solv-N2-opt.run.204360.log
$[Mo_6I_{10}O_2]^{1-}$ *quartet* isomerb 3, O-O clivage	-102.073	-103.599	-100.621	./Mo6I11O2-mI7-1moins-quar-solv-N2-opt.run.205079.log
$[Mo_6I_{10}O_2]^{1-}$ *doublet* isomerb 6, O-O clivage	-102.018	-103.598	-100.564	./I11O2-1moins/Mo6I11O2-mI13-1moins-doub-solv-N2-opt.run.202364.log
$[Mo_6I_{10}O_2]^{1-}$ *quartet* isomerb 4, O-O clivage	-101.929	-103.446	-100.480	./Mo6I11O2-mI8-1moins-quar-solv-N2-opt.run.205081.log
$[Mo_6I_{10}O_2]^{1-}$ *doublet* isomerb 7, O-O clivage	-101.790	-103.244	-100.383	./I11O2-1moins/Mo6I11O2-mI17-1moins-doub-solv-N2-opt.run.204136.log
$[Mo_6I_{10}O_2]^{1-}$ *quartet* isomerb 5, O-O clivage	-101.687	-103.203	-100.263	./Mo6I11O2-mI13-1moins-quar-solv-N2-opt.run.204361.log
$[Mo_6I_{10}O_2]^{1-}$ *quartet* isomerb 6, O-O clivage	-101.572	-103.194	-100.127	./Mo6I11O2-mI11-1moins-quar-solv-N2-opt.run.204357.log
$[Mo_6I_{10}O_2]^{1-}$ *quartet* isomerb 7, O-O clivage	-101.509	-102.968	-100.110	./Mo6I11O2-mI17-1moins-quar-solv-N2-opt.run.204362.log
$[Mo_6I_{10}O_2]^{1-}$ *doublet* isomer 1	-99.245	-100.715	-97.825	./I10O2-1moins/Mo610O2-1moins-doub-Mo6-solv-N2-opt.run.201257.log
$[Mo_6I_{10}O_2]^{1-}$ *doublet* isomer 2	-98.806	-100.244	-97.409	./I10O2-1moins/Mo610O2-1moins-doub-Mo5-solv-N2-opt.run.201256.log
$[Mo_6I_{10}O_2]^{1-}$ *doublet* isomer 3	-98.687	-100.242	-97.239	./I10O2-1moins/Mo610O2-1moins-doub-Mo3-solv-N2-opt.run.201254.log
$[Mo_6I_{10}O_2]^{1-}$ *quartet* isomer 1	-98.624	-100.106	-97.203	./I10O2-1moins/Mo610O2-1moins-quar-Mo6-solv-N2-opt.run.201259.log
$[Mo_6I_{10}O_2]^{1-}$ *quartet* isomer 2	-97.945	-99.479	-96.528	./I10O2-1moins/Mo610O2-1moins-quar-Mo3-solv-N2-opt.run.201261.log
$[Mo_6I_{10}O_2]^{1-}$ *quartet* isomer 3	-97.896	-99.389	-96.476	./I10O2-1moins/Mo610O2-1moins-quar-Mo5-solv-N2-opt.run.201260.log
$[Mo_6I_9]^{1-}$ *singlet* isomer 1	-84.290	-85.854	-83.130	./Mo6I9-1moins-sing-8-solv-N2-opt.run.200909.log
$[Mo_6I_9]^{1-}$ *singlet* isomer 2	-84.146	-85.697	-82.986	./Mo6I9-1moins-sing-12-solv-N2-opt.run.200912.log
$[Mo_6I_9]^{1-}$ *singlet* isomer 3	-84.073	-85.621	-82.913	./Mo6I9-1moins-sing-13-solv-N2-opt.run.200913.log
$[Mo_6I_9]^{1-}$ *singlet* isomer 4	-83.781	-85.340	-82.622	./Mo6I9-1moins-sing-11-solv-N2-opt.run.200911.log
$[Mo_6I_9]^{1-}$ *triplet* isomer 1	-83.717	-85.241	-82.560	./Mo6I9-1moins-trip-7-solv-N2-opt.run.200921.log
$[Mo_6I_9]^{1-}$ *triplet* isomer 2	-83.684	-85.226	-82.528	./Mo6I9-1moins-trip-8-solv-N2-opt.run.200920.log
$[Mo_6I_9]^{1-}$ *singlet* isomer 5	-83.644	-85.132	-82.510	./Mo6I9-1moins-sing-10-solv-N2-opt.run.200910.log
$[Mo_6I_9]^{1-}$ *singlet* isomer 6	-83.605	-85.140	-82.448	./Mo6I9-1moins-sing-7-solv-N2-opt.run.200908.log
$[Mo_6I_9]^{1-}$ *singlet* isomer 7	-83.605	-85.139	-82.448	./Mo6I9-1moins-sing-full-inner-solv-N2-opt.run.201874.log

Please do not adjust margins

$[Mo_6I_9]^{1-}$ *triplet* isomer 3	-83.423	-84.984	-82.267	./Mo6I9-1moins-trip-13-solv-N2-opt.run.200914.log
$[Mo_6I_9]^{1-}$ *triplet* isomer 4	-83.335	-84.945	-82.181	./Mo6I9-1moins-trip-12-solv-N2-opt.run.200916.log
$[Mo_6I_9]^{1-}$ *triplet* isomer 5	-83.242	-84.790	-82.114	./Mo6I9-1moins-trip-11-solv-N2-opt.run.200917.log
$[Mo_6I_9]^{1-}$ *triplet* isomer 6	-83.099	-84.566	-81.996	./Mo6I9-1moins-trip-10-solv-N2-opt.run.200922.log
$[Mo_6I_9]^{1-}$ *triplet* isomer 7	-82.986	-84.515	-81.833	./Mo6I9-1moins-trip-full-inner-solv-N2-opt.run.201803.log
$[Mo_6I_9O_2]^{1-}$ *singlet* isomerb 1, O-O clivage	-99.792	-101.286	-98.416	./Mo6I10O2-mI14-sing-opt.run.212077.log
$[Mo_6I_9O_2]^{1-}$ *singlet* isomer 1, O-O clivage	-99.792	-101.286	-98.416	./Mo6I9O2-1moins-sing-Mo6-solv-N2-opt.run.201585.log
$[Mo_6I_9O_2]^{1-}$ *singlet* isomerb 2, O-O clivage	-99.786	-101.175	-98.460	./Mo6I10O2-mI15-sing-opt.run.212069.log
$[Mo_6I_9O_2]^{1-}$ *singlet* isomerb 3, O-O clivage	-99.572	-101.031	-98.192	./Mo6I10O2-mI13-sing-opt.run.212066.log
$[Mo_6I_9O_2]^{1-}$ *singlet* isomerb 4, O-O clivage	-99.437	-100.915	-98.058	./Mo6I10O2-mI10-sing-opt.run.212063.log
$[Mo_6I_9O_2]^{1-}$ *singlet* isomerb 5, O-O clivage	-99.237	-100.736	-97.860	./Mo6I10O2-mI12-sing-opt.run.212065.log
$[Mo_6I_9O_2]^{1-}$ *singlet* isomerb 6	-95.983	-97.443	-94.619	./Mo6I10O2-mI8-sing-opt.run.214929.log
$[Mo_6I_9O_2]^{1-}$ *singlet* isomerb 7	-95.964	-97.402	-94.599	./Mo6I10O2-mI7-sing-opt.run.212071.log
$[Mo_6I_9O_2]^{1-}$ *singlet* isomerb 8	-95.907	-97.344	-94.541	./Mo6I10O2-mI11-sing-opt.run.212064.log
$[Mo_6I_9O_2]^{1-}$ *singlet* isomerb 9	-95.907	-97.344	-94.541	./Mo6I10O2-mI9-sing-opt.run.214927.log
$[Mo_6I_9O_2]^{1-}$ *triplet* isomerb 1	-95.729	-97.229	-94.361	./Mo6I10O2-mI12-trip-opt.run.214920.log
$[Mo_6I_9O_2]^{1-}$ *triplet* isomer 1	-95.701	-97.127	-94.392	./Mo6I9O2-1moins-trip-Mo6-solv-N2-opt.run.201246.log
$[Mo_6I_9O_2]^{1-}$ *triplet* isomerb 2	-95.698	-97.156	-94.334	./Mo6I10O2-mI7-trip-opt.run.215995.log
$[Mo_6I_9O_2]^{1-}$ *triplet* isomerb 3	-95.682	-97.167	-94.345	./Mo6I10O2-mI14-trip-opt.run.216337.log
$[Mo_6I_9O_2]^{1-}$ *singlet* isomer 2	-95.661	-97.085	-94.316	./Mo6I9O2-1moins-sing-Mo5-solv-N2-opt.run.202095.log
$[Mo_6I_9O_2]^{1-}$ *triplet* isomerb 4	-95.640	-97.065	-94.302	./Mo6I10O2-mI8-trip-opt.run.215986.log
$[Mo_6I_9O_2]^{1-}$ *triplet* isomerb 5	-95.576	-96.976	-94.237	./Mo6I10O2-mI9-trip-opt.run.215988.log
$[Mo_6I_9O_2]^{1-}$ *singlet* isomerb 10	-95.512	-96.982	-94.144	./Mo6I10O2-mI16-sing-opt.run.212070.log
$[Mo_6I_9O_2]^{1-}$ *triplet* isomerb 6	-95.512	-96.967	-94.174	./Mo6I10O2-mI13-trip-opt.run.214921.log
$[Mo_6I_9O_2]^{1-}$ *triplet* isomerb 7	-95.473	-96.856	-94.158	./Mo6I10O2-mI15-trip-opt.run.216152.log
$[Mo_6I_9O_2]^{1-}$ *triplet* isomerb 8	-95.401	-96.772	-94.085	./Mo6I10O2-mI10-trip-opt.run.214918.log
$[Mo_6I_9O_2]^{1-}$ *triplet* isomerb 9	-95.363	-96.753	-94.048	./Mo6I10O2-mI16-trip-opt.run.216151.log
$[Mo_6I_9O_2]^{1-}$ *triplet* isomerb 10	-95.296	-96.709	-93.985	./Mo6I10O2-mI11-trip-opt.run.214919.log
$[Mo_6I_9O_2]^{1-}$ *triplet* isomer 2	-95.189	-96.685	-93.851	./Mo6I9O2-1moins-trip-Mo5-solv-N2-opt.run.201243.log
$[Mo_6I_9O_2]^{1-}$ *triplet* isomer 3	-95.180	-96.683	-93.843	./Mo6I9O2-1moins-trip-Mo4-solv-N2-opt.run.201242.log

This journal is © The Royal Society of Chemistry 20xx

Please do not adjust margins

$[Mo_6I_9O_2]^{1-}$ *singlet* isomer 3	-94.579	-96.085	-93.239	./Mo6I9O2-1moins-sing-Mo4-solv-N2-opt.run.201982.log
$[Mo_6I_8]^{1-}$ *doublet* isomer 1	-80.476	-81.966	-79.397	./Mo6I8-1moins-doub-full-inner-solv-N2-opt.run.201773.log
$[Mo_6I_8]^{1-}$ *doublet* isomer 2	-80.407	-81.868	-79.327	./Mo6I8-1moins-doub-8-solv-N2-opt.run.201236.log
$[Mo_6I_8]^{1-}$ *doublet* isomer 3	-80.296	-81.792	-79.244	./Mo6I8-1moins-doub-10-solv-N2-opt.run.201238.log
$[Mo_6I_8]^{1-}$ *doublet* isomer 4	-80.277	-81.768	-79.225	./Mo6I8-1moins-doub-9-solv-N2-opt.run.201237.log
$[Mo_6I_8]^{1-}$ *doublet* isomer 5	-79.972	-81.418	-78.947	./Mo6I8-1moins-doub-14-solv-N2-opt.run.201239.log
$[Mo_6I_8]^{1-}$ *quartet* isomer 1	-79.817	-81.310	-78.742	./Mo6I8-1moins-quar-7-solv-N2-opt.run.216145.log
$[Mo_6I_8]^{1-}$ *quartet* isomer 2	-79.612	-81.117	-78.565	./Mo6I8-1moins-quar-10-solv-N2-opt.run.216118.log
$[Mo_6I_8]^{1-}$ *quartet* isomer 3	-79.602	-81.124	-78.555	./Mo6I8-1moins-quar-9-solv-N2-opt.run.216147.log
$[Mo_6I_8]^{1-}$ *quartet* isomer 4	-79.433	-80.890	-78.413	./Mo6I8-1moins-quar-14-solv-N2-opt.run.216143.log
$[Mo_6I_8]^{1-}$ *quartet* isomer 5	-79.253	-80.692	-78.203	./Mo6I8-1moins-quar-8-solv-N2-opt.run.216146.log
$[Mo_6I_8]^{1-}$ *quartet* isomer 6	-79.126	-80.563	-78.052	./Mo6I8-1moins-quar-full-inner-solv-N2-opt.run.216148.log
$[Mo_6I_8O]^{1-}$ *doublet* isomer 1	-88.094	-89.545	-86.912	./Mo6I8O-Mo2-1moins-doub-solv-N2-opt.run.204108.log
$[Mo_6I_8O]^{1-}$ *doublet* isomer 2	-87.950	-89.428	-86.767	./Mo6I8O-Mo6-1moins-doub-solv-N2-opt.run.204109.log
$[Mo_6I_8O]^{1-}$ *doublet* isomer 3	-87.788	-89.241	-86.631	./Mo6I8O-Mo4-1moins-doub-solv-N2-opt.run.202725.log
$[Mo_6I_8O]^{1-}$ *quartet* isomer 1	-87.479	-88.916	-86.325	./Mo6I8O-Mo2-1moins-quar-solv-N2-opt.run.216780.log
$[Mo_6I_8O]^{1-}$ *quartet* isomer 2	-87.306	-88.822	-86.127	./Mo6I8O-Mo4-1moins-quar-solv-N2-opt.run.216792.log
$[Mo_6I_8O]^{1-}$ *quartet* isomer 3	-87.306	-88.821	-86.127	./Mo6I8O-Mo5-1moins-quar-solv-N2-opt.run.216803.log
$[Mo_6I_8O]^{1-}$ *quartet* isomer 4	-87.363	-88.818	-86.208	./Mo6I8O-Mo6-1moins-quar-solv-N2-opt.run.216807.log
$[Mo_6I_8O_2]^{1-}$ *doublet* isomerb 1, O-O clivage	-96.595	-97.989	-95.302	./Mo6I9O2-mI12-doub-solv-N2-opt.run.204597.log
$[Mo_6I_8O_2]^{1-}$ *doublet* isomerb 2, O-O clivage	-96.555	-97.935	-95.262	./Mo6I9O2-mI8-doub-solv-N2-opt.run.204593.log
$[Mo_6I_8O_2]^{1-}$ *doublet* isomerb 3, O-O clivage	-96.521	-97.912	-95.249	./Mo6I9O2-mI13-doub-solv-N2-opt.run.205075.log
$[Mo_6I_8O_2]^{1-}$ *doublet* isomerb 4, O-O clivage	-96.450	-97.913	-95.153	./Mo6I9O2-mI11-doub-solv-N2-opt.run.204596.log
$[Mo_6I_8O_2]^{1-}$ *doublet* isomerb 5, O-O clivage	-96.441	-97.843	-95.146	./Mo6I9O2-mI7-doub-solv-N2-opt.run.204592.log
$[Mo_6I_8O_2]^{1-}$ *doublet* isomerb 6, O-O clivage	-96.273	-97.747	-94.979	./Mo6I9O2-mI15-doub-solv-N2-opt.run.204600.log
$[Mo_6I_8O_2]^{1-}$ *doublet* isomerb 7, O-O clivage	-96.263	-97.728	-94.966	./Mo6I9O2-mI10-doub-solv-N2-opt.run.204595.log
$[Mo_6I_8O_2]^{1-}$ *doublet* isomerb 8, O-O clivage	-96.142	-97.492	-94.901	./Mo6I9O2-mI9-doub-solv-N2-opt.run.204594.log

Please do not adjust margins

$[Mo_6I_8O_2]^{1-}$ *quartet* isomerb 1, O-O clivage	-96.049	-97.405	-94.784	./Mo6I9O2-mI12-quar-solv-N2-opt.run.206163.log
$[Mo_6I_8O_2]^{1-}$ *doublet* isomerb 9, O-O clivage	-96.014	-97.353	-94.774	./Mo6I9O2-mI14-doub-solv-N2-opt.run.204599.log
$[Mo_6I_8O_2]^{1-}$ *quartet* isomerb 2, O-O clivage	-95.969	-97.379	-94.704	./Mo6I9O2-mI13-quar-solv-N2-opt.run.205148.log
$[Mo_6I_8O_2]^{1-}$ *quartet* isomerb 3, O-O clivage	-95.958	-97.292	-94.693	./Mo6I9O2-mI8-quar-solv-N2-opt.run.206121.log
$[Mo_6I_8O_2]^{1-}$ *quartet* isomerb 4, O-O clivage	-95.882	-97.300	-94.590	./Mo6I9O2-mI7-quar-solv-N2-opt.run.206122.log
$[Mo_6I_8O_2]^{1-}$ *quartet* isomerb 5, O-O clivage	-95.763	-97.240	-94.474	./Mo6I9O2-mI11-quar-solv-N2-opt.run.205147.log
$[Mo_6I_8O_2]^{1-}$ *quartet* isomerb 6, O-O clivage	-95.666	-97.109	-94.401	./Mo6I9O2-mI10-quar-solv-N2-opt.run.205146.log
$[Mo_6I_8O_2]^{1-}$ *quartet* isomerb 7, O-O clivage	-95.642	-97.088	-94.379	./Mo6I9O2-mI15-quar-solv-N2-opt.run.206123.log
$[Mo_6I_8O_2]^{1-}$ *quartet* isomerb 8, O-O clivage	-95.633	-97.065	-94.368	./Mo6I9O2-mI9-quar-solv-N2-opt.run.205154.log
$[Mo_6I_8O_2]^{1-}$ *quartet* isomerb 9, O-O clivage	-95.626	-96.995	-94.387	./Mo6I9O2-mI14-quar-solv-N2-opt.run.205150.log
$[Mo_6I_8O_2]^{1-}$ *doublet* isomer 1	-92.970	-94.338	-91.681	./I8O2-1moins/Mo6I8O2-1moins-doub-Mo2-solv-N2-opt.run.201984.log
$[Mo_6I_8O_2]^{1-}$ *doublet* isomer 2	-92.239	-93.475	-90.738	./I8O2-1moins/Mo6I8O2-1moins-doub-Mo4-solv-N2-opt.run.201297.log
$[Mo_6I_8O_2]^{1-}$ *doublet* isomer 3	-92.133	-93.397	-90.666	./I8O2-1moins/Mo6I8O2-1moins-doub-Mo5-solv-N2-opt.run.201298.log
Mo6I8O2 1- quartet isomer 1	-92.026	-93.608	-90.981	./I8O2-1moins/Mo6I8O2-1moins-quar-Mo2-solv-N2-opt.run.202369.log
$[Mo_6I_8O_2]^{1-}$ *quartet* isomer 2	-91.955	-93.525	-90.874	./I8O2-1moins/Mo6I8O2-1moins-quar-Mo4-solv-N2-opt.run.202592.log
$[Mo_6I_8O_2]^{1-}$ *quartet* isomer 3	-91.381	-92.848	-90.096	./I8O2-1moins/Mo6I8O2-1moins-quar-Mo5-solv-N2-opt.run.202733.log
$[Mo_6I_7]^{1-}$ *singlet* isomer 1	-76.977	-78.409	-75.976	./Mo6I7-1moins-sing-9-solv-N2-opt.run.201276.log
$[Mo_6I_7]^{1-}$ *singlet* isomer 2	-76.963	-78.400	-75.963	./Mo6I7-1moins-sing-8-solv-N2-opt.run.201275.log
$[Mo_6I_7]^{1-}$ *singlet* isomer 3	-76.949	-78.344	-75.975	./Mo6I7-1moins-sing-14-solv-N2-opt.run.201313.log
$[Mo_6I_7]^{1-}$ *singlet* isomer 4	-76.875	-78.322	-75.874	./Mo6I7-1moins-sing-13-solv-N2-opt.run.201310.log
$[Mo_6I_7]^{1-}$ *singlet* isomer 5	-76.842	-78.269	-75.841	./Mo6I7-1moins-sing-10-solv-N2-opt.run.201277.log
$[Mo_6I_7]^{1-}$ *singlet* isomer 6	-76.837	-78.256	-75.836	./Mo6I7-1moins-sing-12-solv-N2-opt.run.201279.log
$[Mo_6I_7]^{1-}$ *triplet* isomer 1	-76.742	-78.149	-75.744	./Mo6I7-1moins-trip-11-solv-N2-opt.run.201317.log
$[Mo_6I_7]^{1-}$ *singlet* isomer 7	-76.696	-78.125	-75.698	./Mo6I7-1moins-sing-11-solv-N2-opt.run.201278.log
$[Mo_6I_7]^{1-}$ *triplet* isomer 2	-76.617	-78.030	-75.619	./Mo6I7-1moins-trip-full-inner-solv-N2-opt.run.201818.log
$[Mo_6I_7]^{1-}$ *triplet* isomer 3	-76.455	-77.850	-75.457	./Mo6I7-1moins-trip-7-solv-N2-opt.run.201357.log
$[Mo_6I_7]^{1-}$ *triplet* isomer 4	-76.440	-77.853	-75.469	./Mo6I7-1moins-trip-8-solv-N2-opt.run.201356.log
$[Mo_6I_7]^{1-}$ *singlet* isomer 8	-76.424	-77.846	-75.426	./Mo6I7-1moins-sing-7-solv-N2-opt.run.201274.log

This journal is © The Royal Society of Chemistry 20xx

Please do not adjust margins

$[Mo_6I_7]^{1-}$ *triplet* isomer 5	-76.386	-77.867	-75.391	./Mo6I7-1moins-trip-9-solv-N2-opt.run.201319.log
$[Mo_6I_7]^{1-}$ *triplet* isomer 6	-76.235	-77.644	-75.265	./Mo6I7-1moins-trip-10-solv-N2-opt.run.201318.log
$[Mo_6I_7]^{1-}$ *triplet* isomer 7	-76.211	-77.611	-75.241	./Mo6I7-1moins-trip-12-solv-N2-opt.run.201316.log
$[Mo_6I_7]^{1-}$ *triplet* isomer 8	-76.197	-77.637	-75.228	./Mo6I7-1moins-trip-14-solv-N2-opt.run.201314.log
$[Mo_6I_7]^{1-}$ *triplet* isomer 9	-76.144	-77.558	-75.202	./Mo6I7-1moins-trip-13-solv-N2-opt.run.201315.log
$[Mo_6I_7]^{1-}$ *singlet* isomer 9	-75.830	-77.269	-74.835	./Mo6I7-1moins-sing-full-inner-solv-N2-opt.run.201816.log
$[Mo_6I_7O_2]^{1-}$ *singlet* isomer 1, O-O clivage	-92.808	-94.191	-91.596	./Mo6I7O2-1moins-sing-Mo2-solv-N2-opt.run.201446.log
$[Mo_6I_7O_2]^{1-}$ *singlet* isomerb 1	-89.530	-90.853	-88.319	./Mo6I8O2-mI8-sing-opt.run.212078.log
$[Mo_6I_7O_2]^{1-}$ *singlet* isomerb 2	-89.376	-90.683	-88.169	./Mo6I8O2-mI11-sing-opt.run.214938.log
$[Mo_6I_7O_2]^{1-}$ *singlet* isomerb 3	-89.210	-90.547	-88.002	./Mo6I8O2-mI10-sing-opt.run.214936.log
$[Mo_6I_7O_2]^{1-}$ *singlet* isomerb 4	-89.208	-90.506	-88.002	./Mo6I8O2-mI7-sing-opt.run.214946.log
$[Mo_6I_7O_2]^{1-}$ *triplet* isomerb 1	-89.110	-90.414	-87.903	./Mo6I8O2-mI11-trip-opt.run.214948.log
$[Mo_6I_7O_2]^{1-}$ *singlet* isomerb 5	-89.108	-90.358	-87.924	./Mo6I8O2-mI14-sing-opt.run.214944.log
$[Mo_6I_7O_2]^{1-}$ *triplet* isomerb 2	-89.104	-90.470	-87.895	./Mo6I8O2-mI8-trip-opt.run.214956.log
$[Mo_6I_7O_2]^{1-}$ *singlet* isomerb 6	-89.063	-90.403	-87.859	./Mo6I8O2-mI13-sing-opt.run.214942.log
$[Mo_6I_7O_2]^{1-}$ *triplet* isomerb 3	-89.020	-90.407	-87.819	./Mo6I8O2-mI10-trip-opt.run.215998.log
$[Mo_6I_7O_2]^{1-}$ *singlet* isomer 2	-88.967	-90.331	-87.756	./Mo6I7O2-1moins-sing-Mo5-solv-N2-opt.run.201447.log
$[Mo_6I_7O_2]^{1-}$ *triplet* isomer 1	-88.926	-90.267	-87.744	./Mo6I7O2-1moins-trip-Mo2-solv-N2-opt.run.201449.log
$[Mo_6I_7O_2]^{1-}$ *triplet* isomerb 4	-88.818	-90.207	-87.614	./Mo6I8O2-mI13-trip-opt.run.214950.log
$[Mo_6I_7O_2]^{1-}$ *triplet* isomerb 5	-88.816	-90.115	-87.633	./Mo6I8O2-mI14-trip-opt.run.214954.log
$[Mo_6I_7O_2]^{1-}$ *triplet* isomerb 6	-88.813	-90.137	-87.609	./Mo6I8O2-mI7-trip-opt.run.214955.log
$[Mo_6I_7O_2]^{1-}$ *triplet* isomer 2	-88.680	-90.078	-87.474	./Mo6I7O2-1moins-trip-Mo5-solv-N2-opt.run.201448.log
$[Mo_6I_6]^{1-}$ *doublet* isomer 1	-72.938	-74.280	-72.018	./I6-1moins/Mo6I6-1moins-doub-7-solv-N2-opt.run.201431.log
$[Mo_6I_6]^{1-}$ *doublet* isomer 2	-72.841	-74.229	-71.950	./I6-1moins/Mo6I6-1moins-doub-9-solv-N2-opt.run.201433.log
$[Mo_6I_6]^{1-}$ *doublet* isomer 3	-72.784	-74.174	-71.865	./I6-1moins/Mo6I6-1moins-doub-11-solv-N2-opt.run.201434.log
$[Mo_6I_6]^{1-}$ *doublet* isomer 4	-72.752	-74.198	-71.835	./I6-1moins/Mo6I6-1moins-doub-12-solv-N2-opt.run.201435.log
$[Mo_6I_6]^{1-}$ *doublet* isomer 5	-72.670	-74.016	-71.777	./I6-1moins/Mo6I6-1moins-doub-8-solv-N2-opt.run.201432.log
$[Mo_6I_6]^{1-}$ *quartet* isomer 1	-72.325	-73.709	-71.411	./I6-1moins/Mo6I6-1moins-quar-7-solv-N2-opt.run.202734.log
$[Mo_6I_6]^{1-}$ *quartet* isomer 2	-72.151	-73.549	-71.290	./I6-1moins/Mo6I6-1moins-quar-12-solv-N2-opt.run.202740.log
$[Mo_6I_6]^{1-}$ *quartet* isomer 3	-72.132	-73.446	-71.268	./I6-1moins/Mo6I6-1moins-quar-8-solv-N2-opt.run.202735.log
$[Mo_6I_6]^{1-}$ *quartet* isomer 4	-72.092	-73.462	-71.232	./I6-1moins/Mo6I6-1moins-quar-9-solv-N2-opt.run.202738.log
$[Mo_6I_6]^{1-}$ *quartet*	-72.075	-73.475	-71.188	./I6-1moins/Mo6I6-1moins-quar-11-solv-N2-opt.run.202739.log

Please do not adjust margins

isomer 5				
$[Mo_6I_6O_2]^{1-}$ *doublet* isomerb 1	-89.810	-91.060	-88.676	./Mo6I7O2-mI9-1moins-doub-solv-N2-opt.run.204610.log
$[Mo_6I_6O_2]^{1-}$ *doublet* isomerb 2	-89.739	-90.930	-88.629	./Mo6I7O2-mI10-1moins-doub-solv-N2-opt.run.204611.log
$[Mo_6I_6O_2]^{1-}$ *doublet* isomerb 3	-89.658	-90.914	-88.524	./Mo6I7O2-mI12-1moins-doub-solv-N2-opt.run.206199.log
$[Mo_6I_6O_2]^{1-}$ *doublet* isomerb 4	-89.474	-90.802	-88.347	./Mo6I7O2-mI7-1moins-doub-solv-N2-opt.run.205073.log
$[Mo_6I_6O_2]^{1-}$ *doublet* isomerb 5	-89.234	-90.553	-88.133	./Mo6I7O2-mI8-1moins-doub-solv-N2-opt.run.205074.log
$[Mo_6I_6O_2]^{1-}$ *quartet* isomerb 1	-89.202	-90.524	-88.078	./Mo6I7O2-mI7-1moins-quar-solv-N2-opt.run.206204.log
$[Mo_6I_6O_2]^{1-}$ *quartet* isomerb 2	-89.198	-90.444	-88.128	./Mo6I7O2-mI8-1moins-quar-solv-N2-opt.run.206207.log
$[Mo_6I_6O_2]^{1-}$ *quartet* isomerb 3	-89.035	-90.304	-87.936	./Mo6I7O2-mI10-1moins-quar-solv-N2-opt.run.206193.log
$[Mo_6I_6O_2]^{1-}$ *doublet* isomerb 6	-88.940	-90.302	-87.810	./Mo6I7O2-mI13-1moins-doub-solv-N2-opt.run.204614.log
$[Mo_6I_6O_2]^{1-}$ *quartet* isomerb 4	-88.896	-90.231	-87.797	./Mo6I7O2-mI9-1moins-quar-solv-N2-opt.run.206209.log
$[Mo_6I_6O_2]^{1-}$ *doublet* isomerb 7	-88.620	-89.945	-87.491	./Mo6I7O2-mI11-1moins-doub-solv-N2-opt.run.204612.log
$[Mo_6I_6O_2]^{1-}$ *quartet* isomerb 5	-88.575	-89.931	-87.445	./Mo6I7O2-mI12-1moins-quar-solv-N2-opt.run.207449.log
$[Mo_6I_6O_2]^{1-}$ *quartet* isomerb 6	-88.493	-89.777	-87.393	./Mo6I7O2-mI11-1moins-quar-solv-N2-opt.run.206197.log
$[Mo_6I_6O_2]^{1-}$ *quartet* isomerb 7	-88.490	-89.854	-87.394	./Mo6I7O2-mI13-1moins-quar-solv-N2-opt.run.206203.log
$[Mo_6I_5]^{1-}$ *singlet* isomer 1	-69.433	-70.727	-68.591	./Mo6I5-1moins-sing-12-solv-N2-opt.run.201811.log
$[Mo_6I_5]^{1-}$ *singlet* isomer 2	-69.425	-70.712	-68.583	./Mo6I5-1moins-sing-8-solv-N2-opt.run.201762.log
$[Mo_6I_5]^{1-}$ *singlet* isomer 3	-69.236	-70.488	-68.393	./Mo6I5-1moins-sing-10-solv-N2-opt.run.201764.log
$[Mo_6I_5]^{1-}$ *singlet* isomer 4	-69.056	-70.351	-68.215	./Mo6I5-1moins-sing-11-solv-N2-opt.run.201765.log
$[Mo_6I_5]^{1-}$ *singlet* isomer 5	-68.916	-70.192	-68.075	./Mo6I5-1moins-sing-7-solv-N2-opt.run.201761.log
$[Mo_6I_5]^{1-}$ *triplet* isomer 1	-68.801	-70.061	-67.963	./Mo6I5-1moins-trip-9-solv-N2-opt.run.202117.log
$[Mo_6I_5]^{1-}$ *singlet* isomer 6	-68.790	-70.044	-67.950	./Mo6I5-1moins-sing-9-solv-N2-opt.run.201763.log
$[Mo_6I_5]^{1-}$ *triplet* isomer 2	-68.726	-70.099	-67.890	./Mo6I5-1moins-trip-11-solv-N2-opt.run.202120.log
$[Mo_6I_5]^{1-}$ *triplet* isomer 3	-68.714	-70.063	-67.879	./Mo6I5-1moins-trip-12-solv-N2-opt.run.202122.log
$[Mo_6I_5]^{1-}$ *triplet* isomer 4	-68.638	-69.999	-67.803	./Mo6I5-1moins-trip-8-solv-N2-opt.run.202116.log
$[Mo_6I_5]^{1-}$ *triplet* isomer 5	-68.609	-69.924	-67.773	./Mo6I5-1moins-trip-10-solv-N2-opt.run.202118.log
$[Mo_6I_5]^{1-}$ *triplet* isomer 6	-68.506	-69.830	-67.670	./Mo6I5-1moins-trip-7-solv-N2-opt.run.202115.log

This journal is © The Royal Society of Chemistry 20xx

Please do not adjust margins

Table S4 - Gibbs free energies ($\Delta G_{298\ K}$) and enthalpies ($\Delta H_{298\ K}$) at 298 K of the indicated reaction.

Gibbs free energies ($\Delta G_{298\ K}$) and enthalpies ($\Delta H_{298\ K}$) at 298 K of the indicated reaction. The geometry of the reactants $[Mo_6I_n]^-$ and $[Mo_6I_nO_2]^-$ are the most stable isomers that are obtained following the procedure detailed in the caption of Table Theo 1. The $[Mo_6I_{(n-1)}O_2]^-$ isomers issued from the $[Mo_6I_nO_2]^-$ (n = 13-6) are differentiated by the letter b added to isomer (isomers b).

Reactions: $[Mo_6I_n]^{x-}$ > $[Mo_6I_{n-1}]^{x\ or\ (x-1)-}$ + $I^{\bullet}$ or 1-	$\Delta E_{SCM-ADF}$ (eV)	ΔG_{298K} (eV)	$\Delta H_{298\ K}$ (eV)
$[Mo_6I_{14}]^{2-}$ > $[Mo_6I_{13}]^{2-}$ + $I^{\bullet}$	3.490	3.540	3.408
$[Mo_6I_{14}]^{2-}$ > $[Mo_6I_{13}]^{-}$ + I^{-}	0.735	0.848	0.632
$[Mo_6I_{14}]^{-}$ -> $[Mo_6I_{13}]^{-}$ + $I^{\bullet}$	1.933	1.989	1.911
$[Mo_6I_{13}]^{-}$ -> $[Mo_6I_{12}]^{-}$ + $I^{\bullet}$	2.979	3.040	2.898
$[Mo_6I_{12}]^{-}$ -> $[Mo_6I_{11}]^{-}$ + $I^{\bullet}$	3.028	3.053	2.949
$[Mo_6I_{11}]^{-}$ -> $[Mo_6I_{10}]^{-}$ + $I^{\bullet}$	3.192	3.245	3.110
$[Mo_6I_{10}]^{-}$ -> $[Mo_6I_{9}]^{-}$ + $I^{\bullet}$	2.753	2.794	2.676
$[Mo_6I_{9}]^{-}$ -> $[Mo_6I_{8}]^{-}$ + $I^{\bullet}$	3.562	3.635	3.480
$[Mo_6I_{8}]^{-}$ -> $[Mo_6I_{7}]^{-}$ + $I^{\bullet}$	3.247	3.305	3.169
$[Mo_6I_{7}]^{-}$ -> $[Mo_6I_{6}]^{-}$ + $I^{\bullet}$	3.787	3.877	3.705
$[Mo_6I_{6}]^{-}$ -> $[Mo_6I_{5}]^{-}$ + $I^{\bullet}$	3.252	3.300	3.175

Reaction: $[Mo_6I_n]^{-/2-}$ + O_2 -> $[Mo_6I_nO_2]^{-/2-}$	$\Delta E_{SCM-ADF}$ (eV)	$\Delta G_{SCM-ADF}$ (eV)	$\Delta H_{SCM-ADF}$ (eV)
$[Mo_6I_{13}]^{2-}$ + O_2 -> $[Mo_6I_{13}O_2]^{2-}$	-1.694	-1.221	-1.659
$[Mo_6I_{13}]^{-}$ + O_2 -> $[Mo_6I_{13}O_2]^{-}$ *triplet*	-0.496	-0.027	-0.530
$[Mo_6I_{13}]^{-}$ + O_2 -> $[Mo_6I_{13}O_2]^{-}$ *singlet*	-0.393	0.082	-0.365
$[Mo_6I_{12}]^{-}$ + O_2 -> $[Mo_6I_{12}O_2]^{-}$	-1.369	-0.949	-1.343
$[Mo_6I_{11}]^{-}$ + O_2 -> $[Mo_6I_{11}O_2]^{-}$	-5.249	-4.828	-5.213
$[Mo_6I_{10}]^{-}$ + O_2 -> $[Mo_6I_{10}O_2]^{-}$	-2.158	-1.737	-2.160
$[Mo_6I_{9}]^{-}$ + O_2 -> $[Mo_6I_{9}O_2]^{-}$	-5.711	-5.290	-5.679
$[Mo_6I_{8}]^{-}$ + O_2 -> $[Mo_6I_{8}O_2]^{-}$	-1.971	-1.550	-1.977
$[Mo_6I_{7}]^{-}$ + O_2 -> $[Mo_6I_{7}O_2]^{-}$	-6.040	-5.619	-6.013

Reaction leading to isomer b of $[Mo_6I_{12}O_2]^{-}$	$\Delta E_{SCM-ADF}$ (eV)	$\Delta G_{SCM-ADF}$ (eV)	$\Delta H_{SCM-ADF}$ (eV)
$[Mo_6I_{13}O_2]^{-}$ -> $[Mo_6I_{12}O_2]^{-}$ + $I^{\bullet}$ *triplet*	2.106	2.170	2.085
$[Mo_6I_{13}O_2]^{-}$ -> $[Mo_6I_{12}O_2]^{-}$ + $I^{\bullet}$ *singlet*	2.002	2.061	1.920
$[Mo_6I_{12}O_2]^{-}$ -> $[Mo_6I_{11}O_2]^{-}$ + $I^{\bullet}$	2.747	2.839	2.639
$[Mo_6I_{11}O_2]^{-}$ -> $[Mo_6I_{10}O_2]^{-}$ + $I^{\bullet}$	2.642	2.678	2.556
$[Mo_6I_{10}O_2]^{-}$ -> $[Mo_6I_{9}O_2]^{-}$ + $I^{\bullet}$	-0.800	-0.823	-0.844
$[Mo_6I_{9}O_2]^{-}$ -> $[Mo_6I_{8}O_2]^{-}$ + $I^{\bullet}$	2.945	3.045	2.861
$[Mo_6I_{8}O_2]^{-}$ -> $[Mo_6I_{7}O_2]^{-}$ + $I^{\bullet}$	2.457	2.457	2.456
$[Mo_6I_{7}O_2]^{-}$ -> $[Mo_6I_{6}O_2]^{-}$ + $I^{\bullet}$	2.746	2.878	2.667

Figures

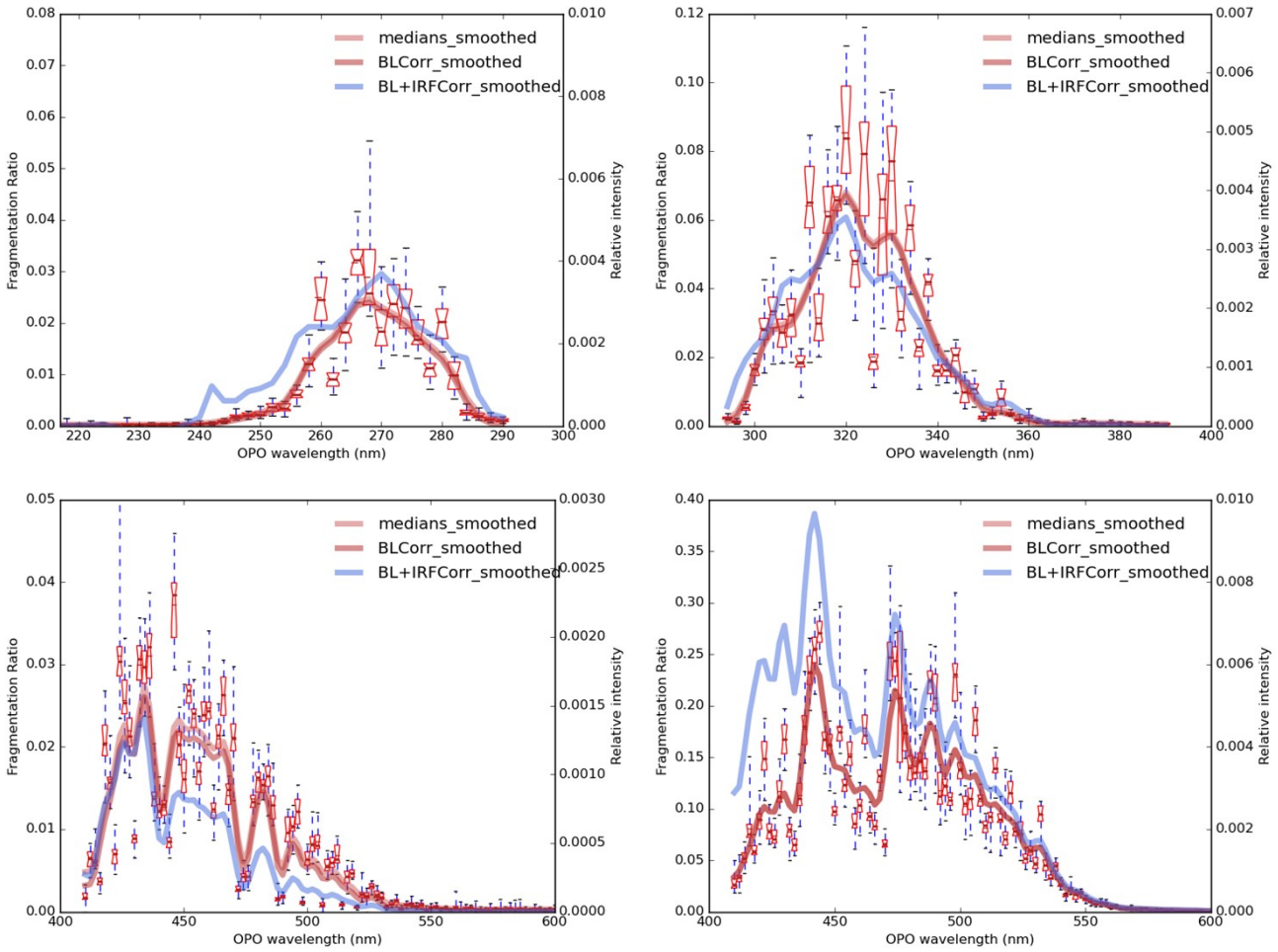

Figure S0. Data analysis workflow for each wavelength range of acquisition: the fragmentation ratios (boxplots) are statistically analysed and medians are baseline corrected, then smoothed and ultimately corrected for the laser profile (divided by power*wavelength which is called here “instrument response function” or IRF). This workflow is applied to the 2 UV ranges and 2 replicates in the Visible range.

This journal is © The Royal Society of Chemistry 20xx

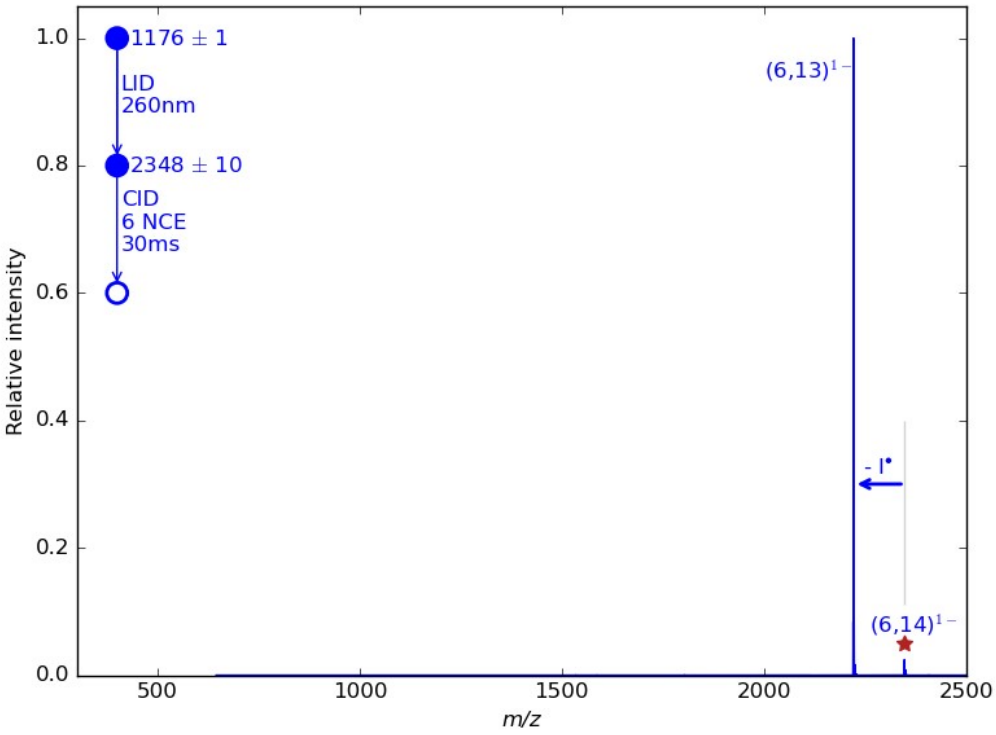

Figure S1. CID spectrum of $[Mo_6I_{14}]^{1-}$ at *m/z* 2348 (formed by LID of precursor $[Mo_6I_{14}]^{2-}$). The exclusive activation product is marked with thick blue arrows and corresponds to the loss of radical iodine I•.

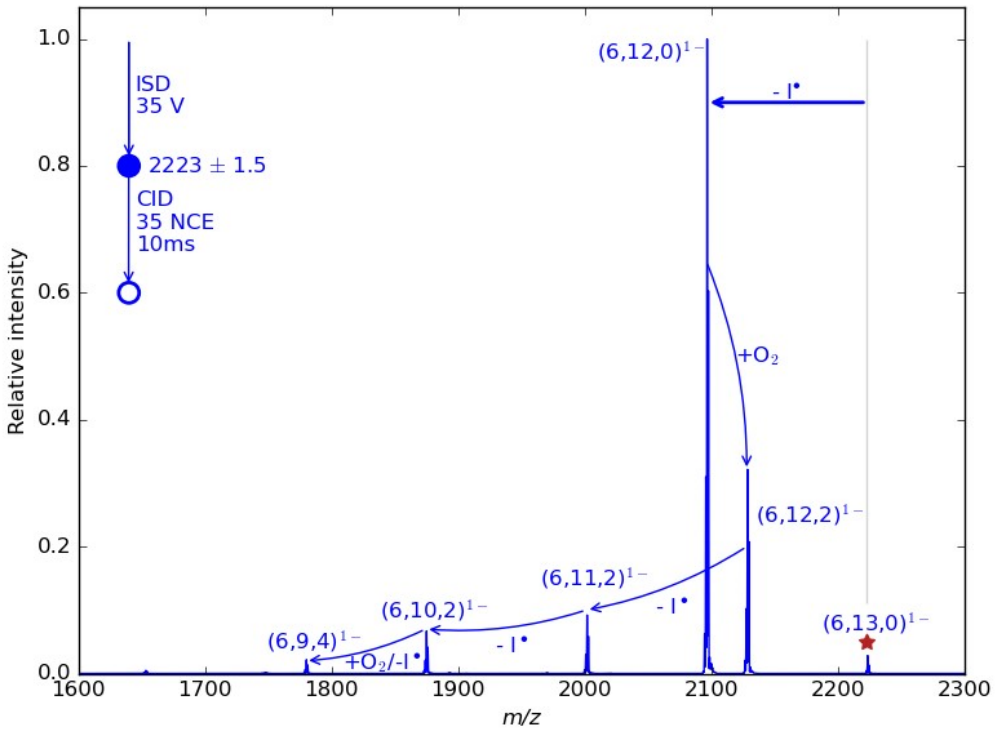

Figure S2. CID spectrum of $[Mo_6I_{13}]^{1-}$ at *m/z* 2223 (formed by ISD after ESI of a solution of $Cs_2Mo_6I_{14}$).

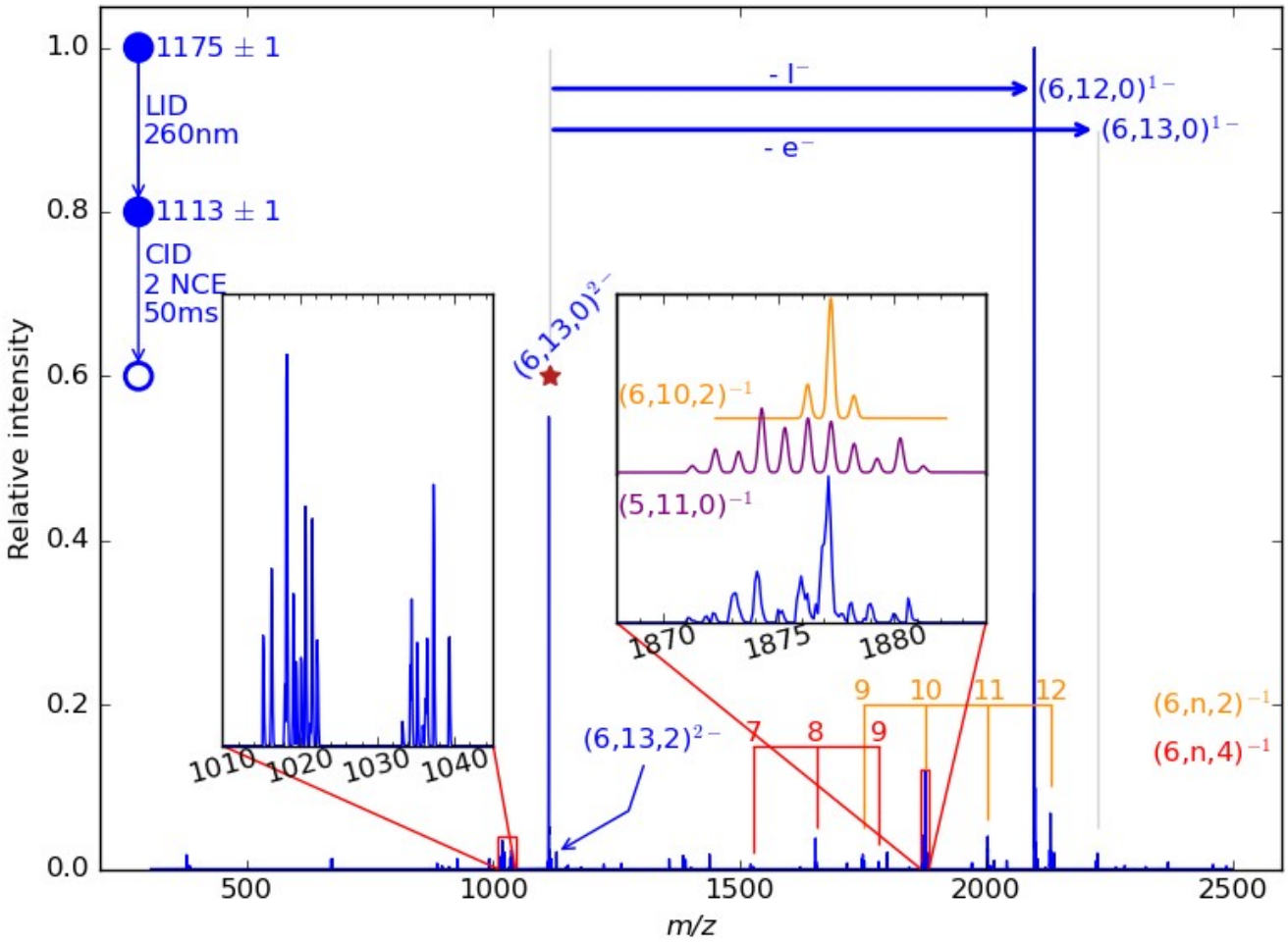

Figure S3. CID spectrum of $[Mo_6I_{13}]^{2-\bullet}$ at *m/z* 1112 (formed by LID of precursor $[Mo_6I_{14}]^{2-}$. Primary activation products are marked with thick blue arrows. Secondary fragment series resulting from O_2 addition and I• losses are indicated with orange and red scales. Mo_6 core fragmentation is observed as attested by several complex patterns in insets (the small isolation window enables to simulate exact patterns for specific neutral losses: see orange/purple patterns in inset).

Figure S3 description: Multiple features can be noted in this MS^3 spectrum.

- First, the most intense fragment corresponds to the $(6,12,0)^{1-}$ mono-anion, at *m/z* 2098, formed by I^- loss. This fragment is also the most abundant by CID of $(6,13,0)^{1-}$ although it appears at much higher collisional energy (see Figure S5). Thus, fragmentation of the dianion may be an alternative, low energy formation path for $(6,12,0)^{1-}$ in Figure 1 that does not require the oxidized species $(6,14,0)^{1-}$. Species $(6,12,0)^{1-}$ may in turn react with O_2 to form $(6,12,2)^{1-}$ at *m/z* 2130, and associated I• loss product $(6,11,2)^{1-}$ at *m/z* 2003. However, the observed yields are relatively low (respectively 7% and 4% of $(6,12,0)^{1-}$ during the 50 ms activation time). This is in line with observations from Figures 1 and 2 where the $(6,12,0)^{1-}$ species lays only at the onset of reactivity with O_2 traces.
- Second, the $(6,13,0)^{1-}$ mono-anion is observed at *m/z* 2225. The release of an electron with nearly no activation energy is another sign of the instability of this electron-rich species.
- Third, although yields are very low (< 5% of precursor), the reduced $(6,13,0)^{2-}$ di-anion reacts with O_2, similarly **to what was observed for $[Mo_6I_n]^{1-}$ ions (n < 13),** to form the $(6,13,2)^{2-}$ cluster at *m/z* 1128 and the associated I• loss product $(6,12,2)^{2-}$ at *m/z* 1064.

This journal is © The Royal Society of Chemistry 20xx

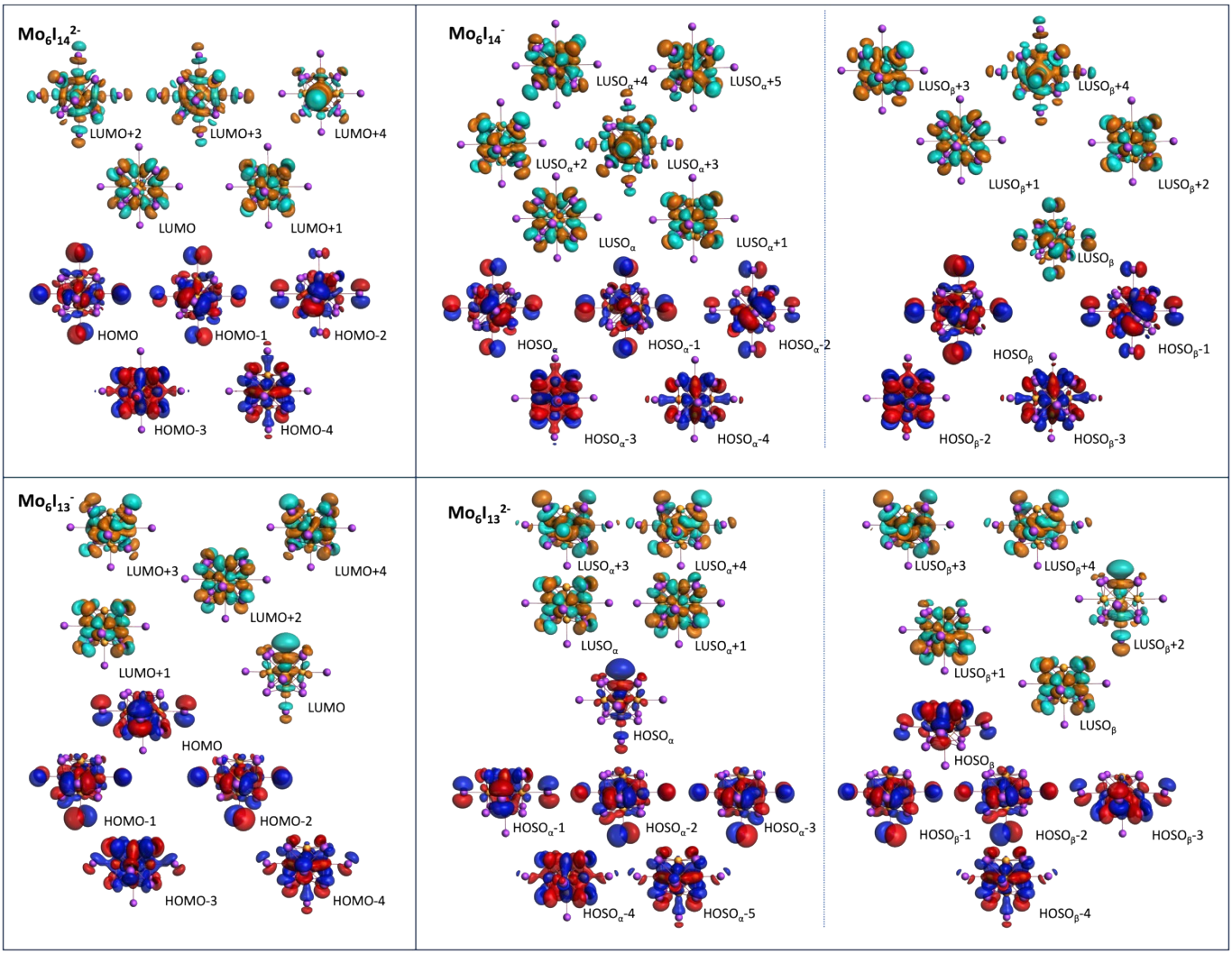

Figure S4. The representation of the frontier MOs of (Spin)orbital of $[Mo_6I_{14}]^{2-}$, $[Mo_6I_{14}]^{1-\bullet}$, $[Mo_6I_{13}]^{2-\bullet}$, and $[Mo_6I_{13}]^{-}$. The corresponding molecular energy diagrams are given in Figure 2 in the main text. = HOMO = highest occupied molecular orbitals; $HOSO_\alpha$ / $HOSO_\beta$ = highest occupied spin orbital α / β; LUMO = lowest unoccupied molecular orbital; $LUSO_\alpha$ / $LUSO_\beta$ = = lowest unoccupied spin orbital α / β. Isocontours = ±0.02 $(e.bohr^3)^{½}$.

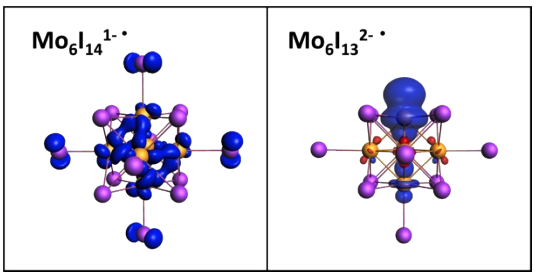

Figure S5. Spin-density representation of $[Mo_6I_{14}]^{1-\bullet}$ and $[Mo_6I_{13}]^{2-\bullet}$. Isocontours = ±0.0025 $e.bohr^3$.

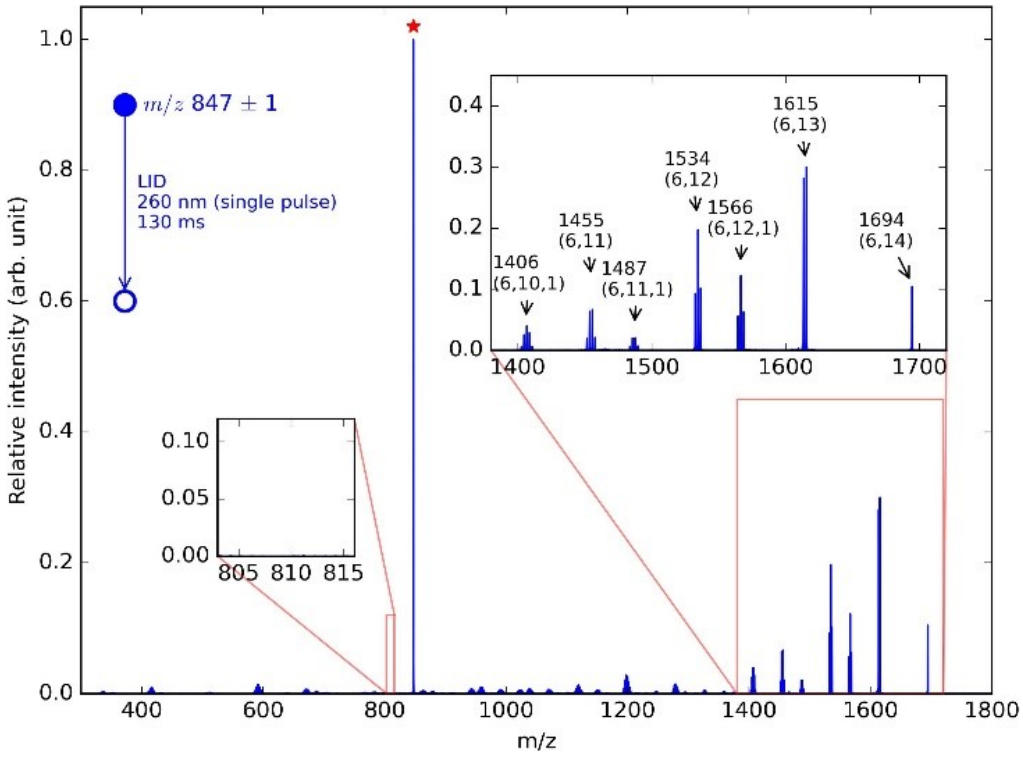

Figure S6. Photo-fragmentation spectrum (LID) at 260 nm of a single isotopic peak (*m/z* 847) of the precursor ion $Mo_6Br_{14}^{2-}$. LID mainly yields singly charged fragments resulting either from the electron photo-detachment or from the loss of I^-, both followed by successive I_2 losses. In comparison with the iodinated compound, the reduced dianion species $(6,13,0)^{2-\bullet}$ is not detected at *m/z* 807.

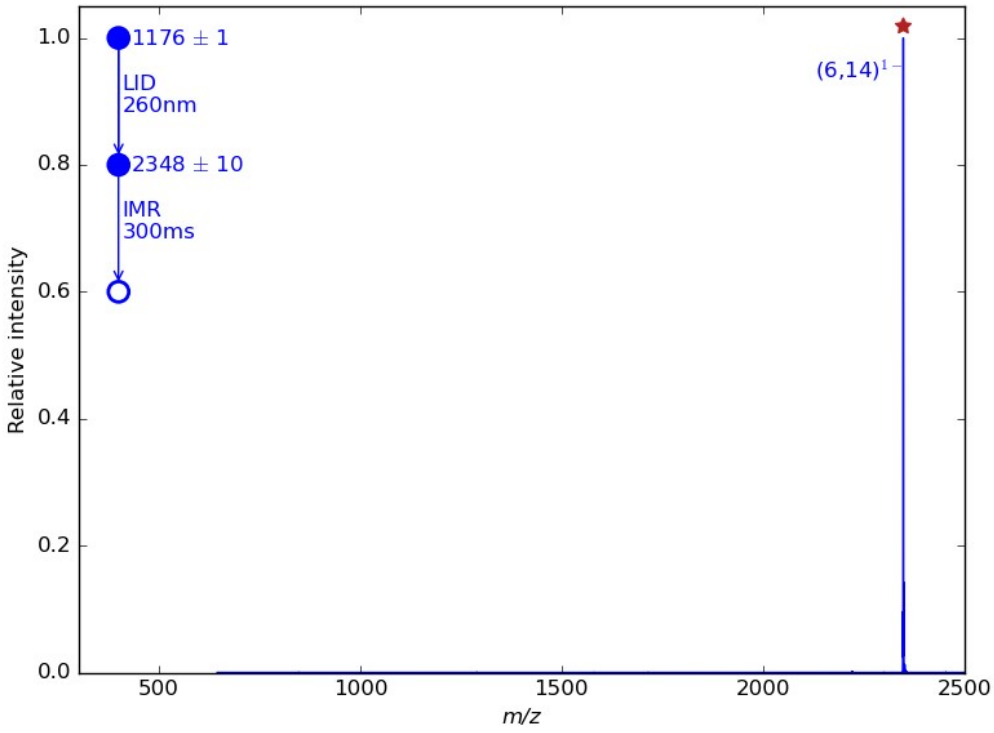

Figure S7. IMR spectrum of $[Mo_6I_{14}]^{1-}$ at *m/z* 2348 (formed by LID of precursor $[Mo_6I_{14}]^{2-}$). No product is formed from reaction with trace O_2 (see Figure 7 for comparison with reactivity of (6,13,0)2- under similar conditions).

This journal is © The Royal Society of Chemistry 20xx

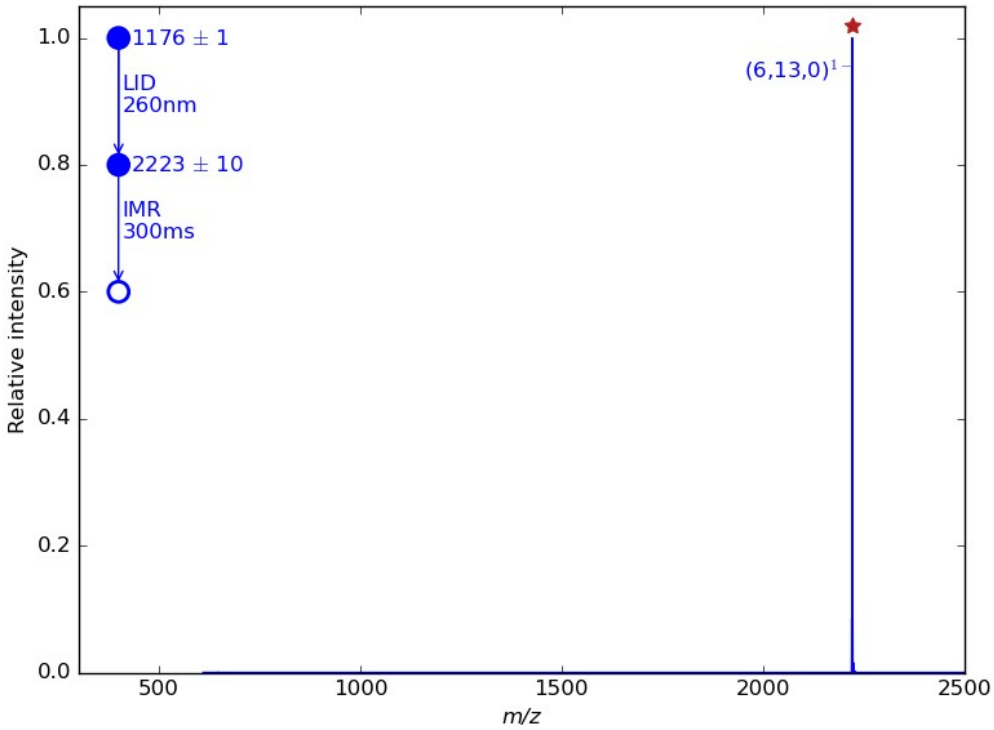

Figure S8. IMR spectrum of $[Mo_6I_{13}]^{1-}$ at *m/z* 2223 (formed by LID of precursor $[Mo_6I_{14}]^{2-}$). No product is formed from reaction to trace O_2 (see Figure 7 for comparison with reactivity of (6,13,0)2- under similar conditions).

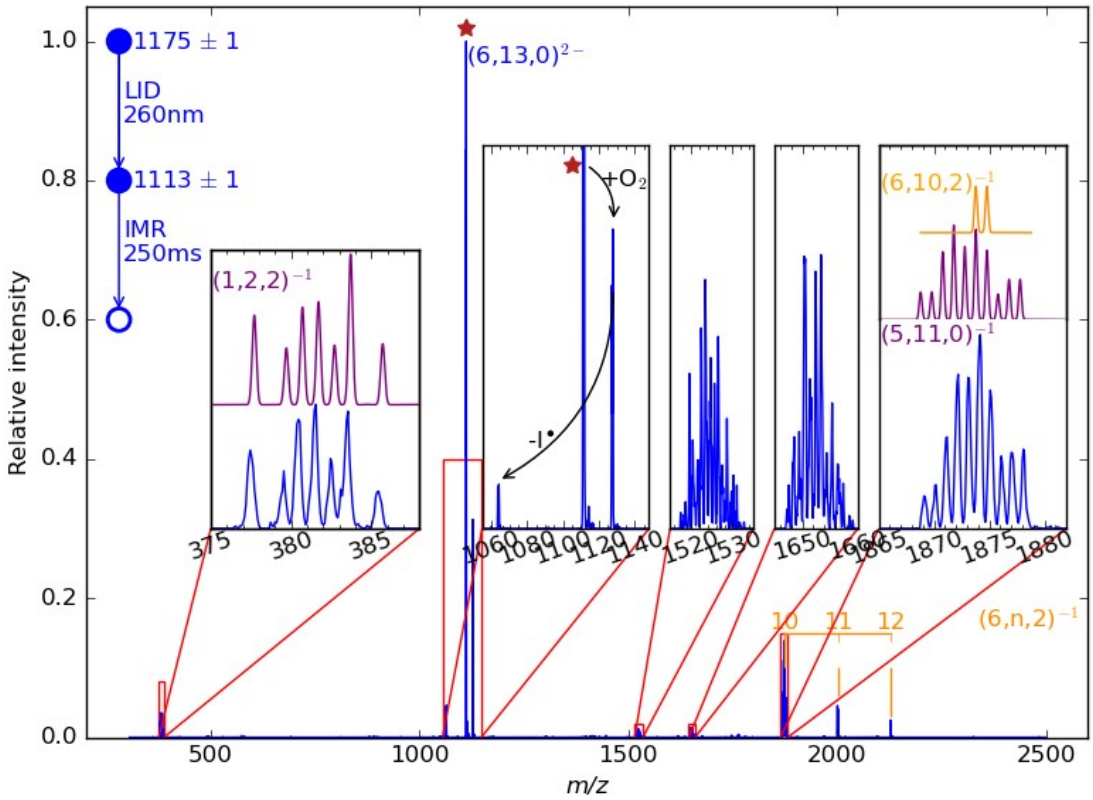

Figure S9. Evolution of the photo-product ion $[Mo_6I_{13}]^{2-}$ (marked with asterix) after 250 ms in the trap background gas (He with unavoidable traces of O_2). Insets show ion series that all derive from an initial O_2 addition. Left and right insets display simulated isotope patterns in purple or orange for respectively $[MoI_2O_2]^{1-}$ and [selected precursor *m/z* - $MoI_2O_2]^{1-}$ or $[Mo_6I_{10}O_2]^{1-}$.

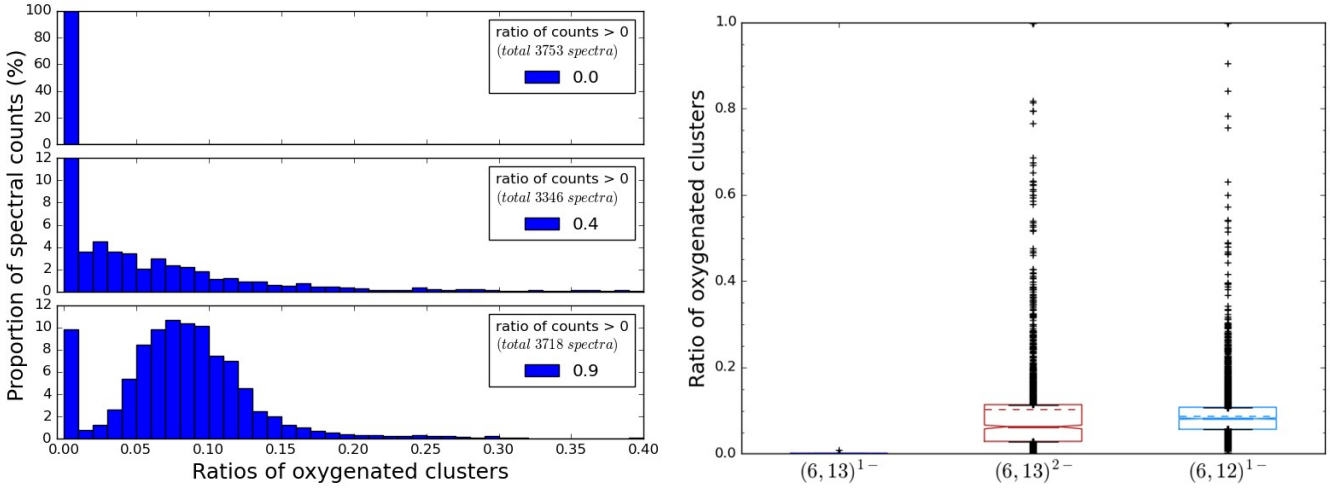

Figure S10. Analysis of the oxidation ratio of clusters with 13 or 12 iodines. (Left) Comparison of the spectral count distributions for $(6,13,0)^{1-}$ (top) vs. $(6,13,0)^{2-\bullet}$ (middle) and $(6,12,0)^{1-\bullet}$ (bottom). Data is presented as relative ion counts per bin calculated over more than 3000 mass spectra recorded within the mid-UV, near-UV and visible absorption bands of $(6,14,0)^{1-}$ (see Figure 3 in the manuscript). While $(6,13,x)^{1-}$ displays systematically strict zero ratios, a bi-modal distribution is observed for$(6,13,x)^{2-\bullet}$ which is comparable to $(6,12,x)^{1-\bullet}$, as shown on the boxplot representation displaying the position of quartiles and outliers after filtering off for all species the strict zeros (Right).

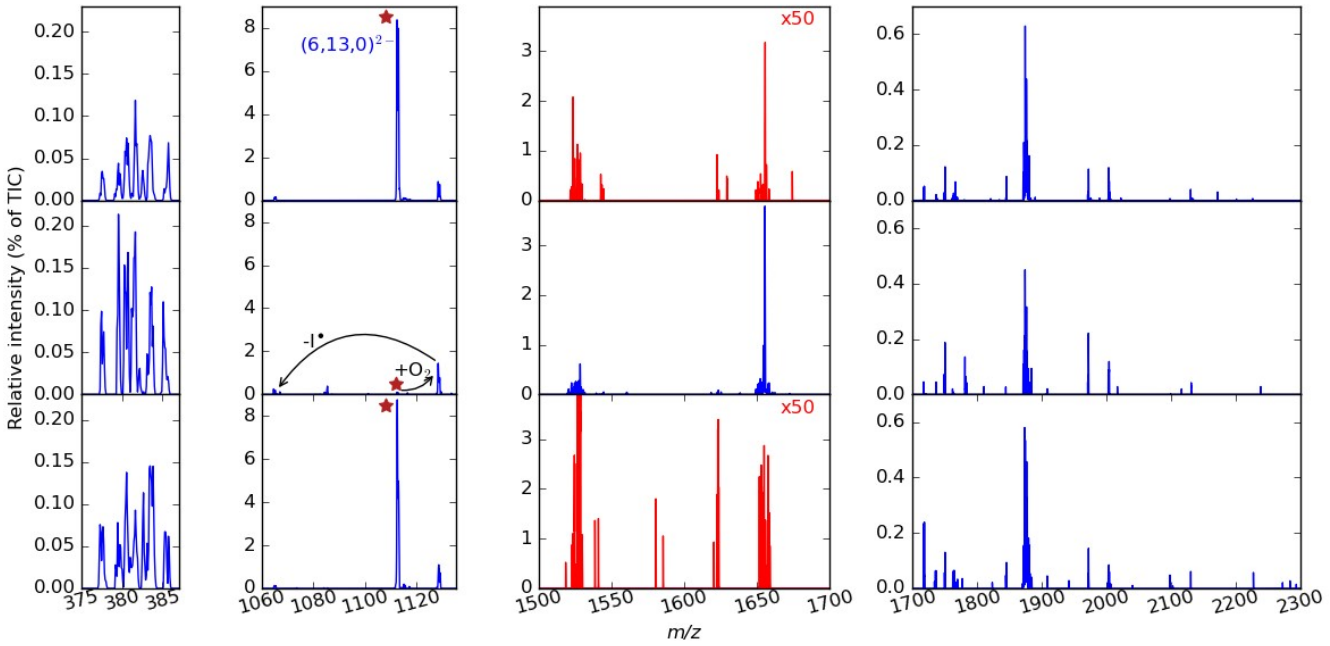

Figure S11. Reactivity of $(6,13,0)^{2-}$ at *m/z* 1112 with trap background gas. Top: Helium (with unavoidable traces of O_2); middle: He:O_2(0.5%); and bottom: He:CO_2(0.5%).

This journal is © The Royal Society of Chemistry 20xx

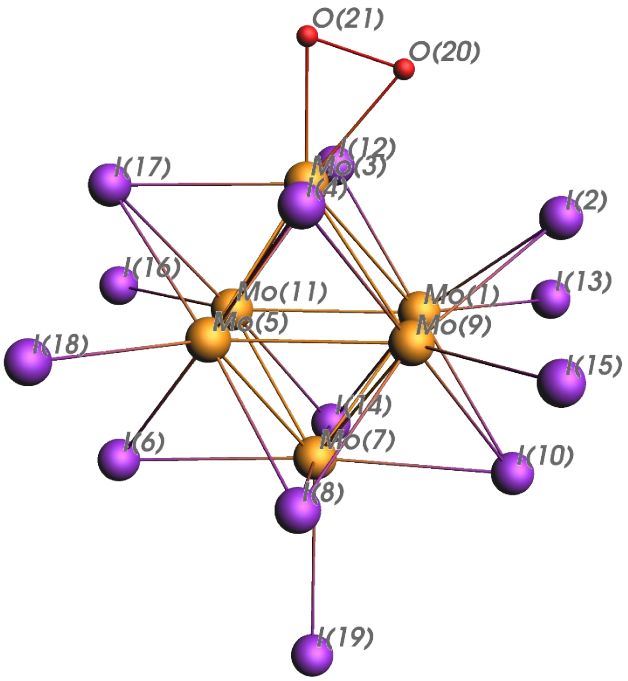

Bond	Length (Å)
O(20)-O(21)	1.395
Mo(3)-O(20)	2.063
Mo(3)-O(21)	2.018
Mo(3)-Mo(9)	2.828
Mo(3)-Mo(5)	2.677
Mo(3)-Mo(11)	2.676
Mo(3)-Mo(1)	2.828
Mo(7)-Mo(1)	2.691
Mo(7)-Mo(9)	2.670
Mo(7)-Mo(5)	2.670
Mo(7)-Mo(11)	2.691
Mo(1)-Mo(9)	2.639
Mo(9)-Mo(5)	2.727
Mo(5)-Mo(11)	2.680
Mo(11)-Mo(1)	2.728
Mo(3)-I(2)	3.531
Mo(3)-I(4)	2.793
Mo(3)-I(17)	2.746
Mo(3)-I(12)	2.792
Mo(7)-I(19)	2.889
Mo(7)-I(10)	2.778
Mo(7)-I(8)	2.793

Bond	Length (Å)
Mo(7)-I(6)	2.795
Mo(7)-I(14)	2.793
Mo(9)-I(15)	2.910
Mo(9)-I(2)	2.837
Mo(9)-I(4)	2.808
Mo(9)-I(10)	2.800
Mo(9)-I(8)	2.814
Mo(5)-I(18)	2.884
Mo(5)-I(4)	2.816
Mo(5)-I(17)	2.814
Mo(5)-I(8)	2.785
Mo(5)-I(6)	2.800
Mo(11)-I(16)	2.884
Mo(11)-I(17)	2.814
Mo(11)-I(12)	2.817
Mo(11)-I(6)	2.800
Mo(11)-I(14)	2.785
Mo(1)-I(13)	2.910
Mo(1)-I(12)	2.808
Mo(1)-I(2)	2.838
Mo(1)-I(14)	2.814
Mo(1)-I(10)	2.800

Figure S12. Representation of the optimized geometry of (6,13,2)2-• and list of the interatomic distances.

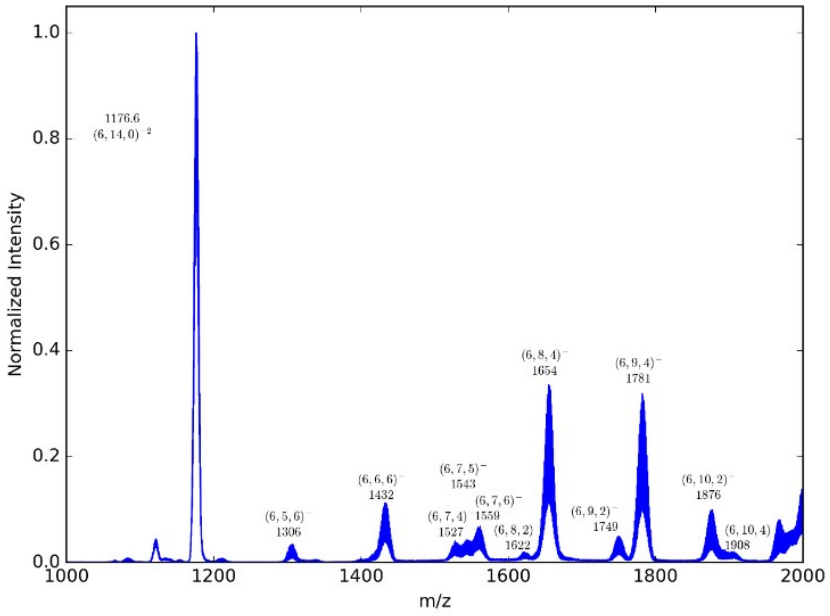

Figure S13. In source CID (35 V) of $(6,14,0)^{2-}$ in presence of 0.5% CO_2 in the trapping gas. Major fragments correspond to $(6,n,2k)^{1-}$ species similar to what is observed with O_2 traces. No CO_2 adduct peak is directly identified. However, some *odd* oxygens ions are observed, *e.g.* at *m/z* 1543.

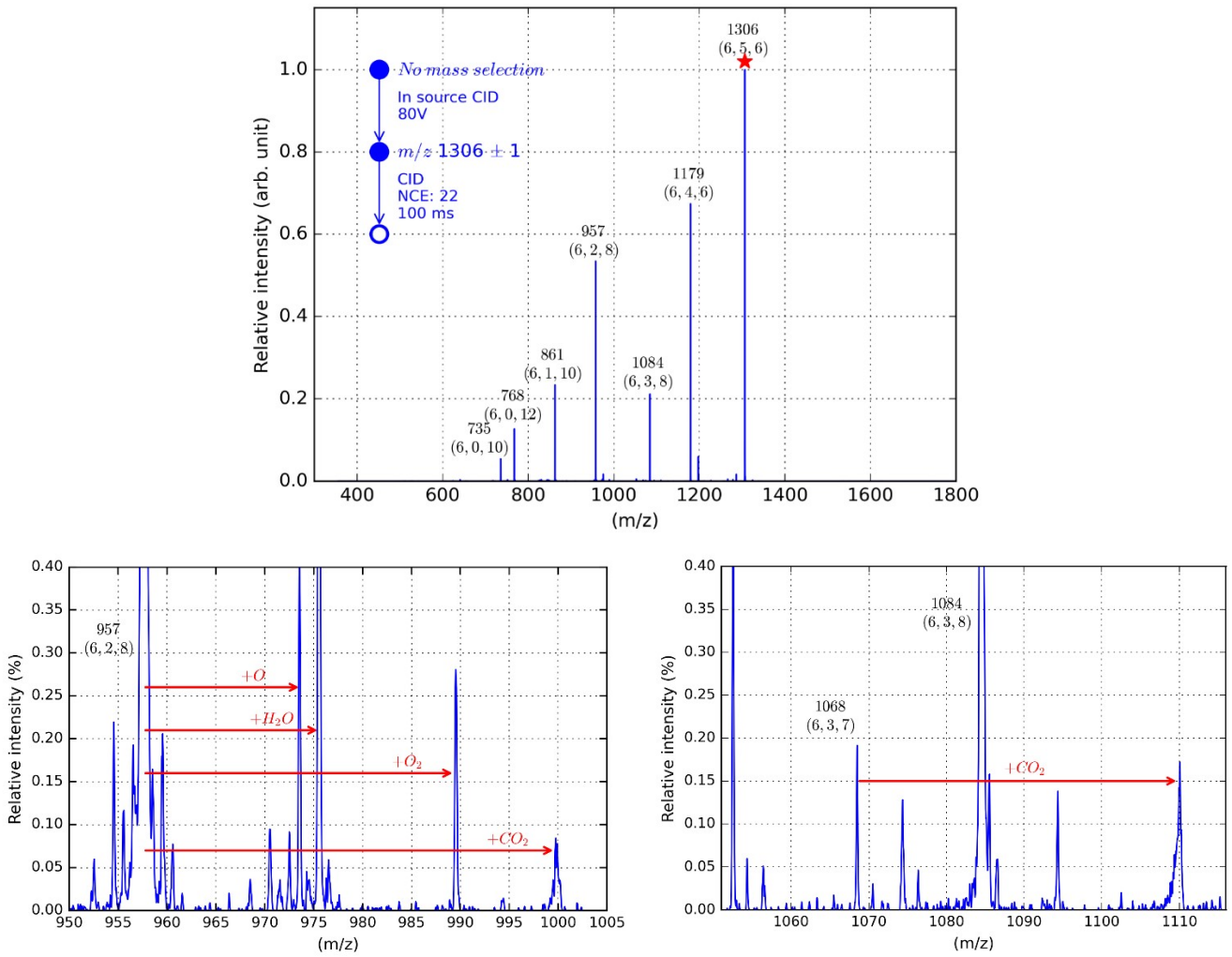

Figure S14. CID-MS^2 spectrum of precursor species $(6,5,6)^{1-}$ formed by in-source CID (80 V) and isolated at m/z 1306. Collisional activation (NCE 22) was applied during 100 ms in the presence of CO_2 seeded at 0.5% in the helium-trapping gas. Major fragments correspond to $(6,n,2k)^{1-}$ species similar to what is observed with O_2 traces. No CO_2 adduct peak is directly identified. However, some mis-shaped minor peaks are observed at m/z 999.8 and 1110.1 about 42 Th above ions $(6,3,7)^{1-}$ and $(6,2,8)^{1-}$. Under the assumption that the peak fronting is associated with the detection of metastable ions, it is likely that these peaks correspond to fragile CO_2 adducts detected at lower *m/z* due to dissociation during detection.

This journal is © The Royal Society of Chemistry 20xx